



## INORGANIC IONS SENSING BY SURFACE-ENHANCED RAMAN SCATTERING SPECTROSCOPY.

Dionysia Tsoutsi

Dipòsit Legal: T 554-2015

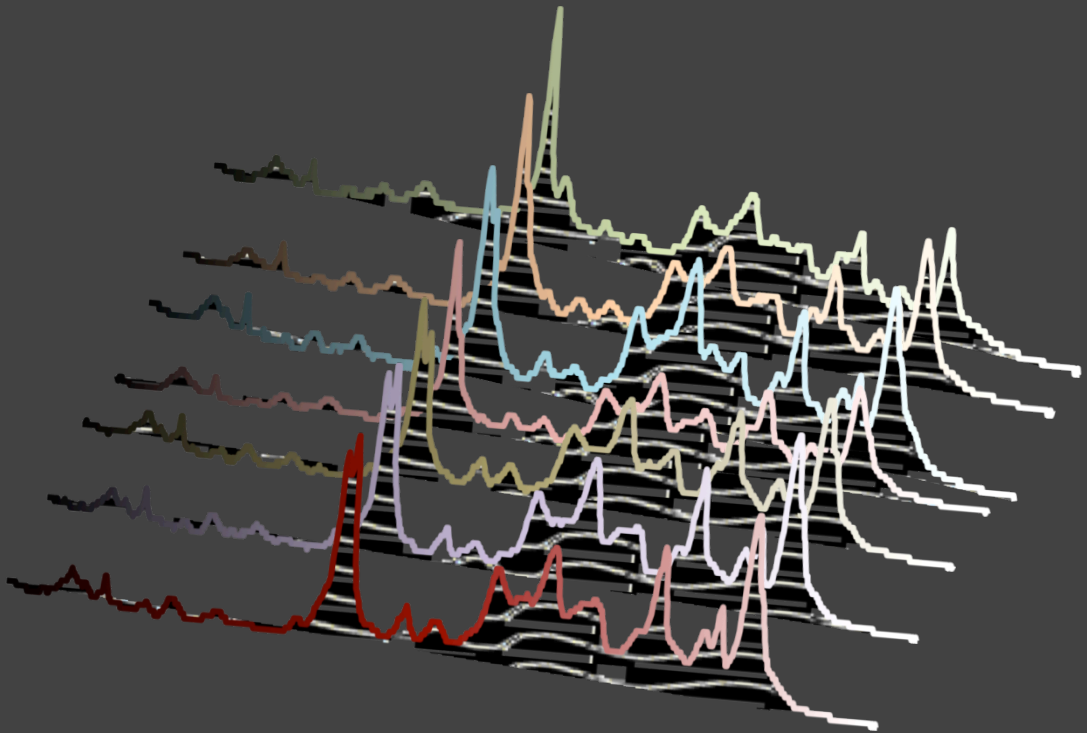
**ADVERTIMENT.** L'accés als continguts d'aquesta tesi doctoral i la seva utilització ha de respectar els drets de la persona autora. Pot ser utilitzada per a consulta o estudi personal, així com en activitats o materials d'investigació i docència en els termes establerts a l'art. 32 del Text Refós de la Llei de Propietat Intel·lectual (RDL 1/1996). Per altres utilitzacions es requereix l'autorització prèvia i expressa de la persona autora. En qualsevol cas, en la utilització dels seus continguts caldrà indicar de forma clara el nom i cognoms de la persona autora i el títol de la tesi doctoral. No s'autoritza la seva reproducció o altres formes d'explotació efectuades amb finalitats de lucre ni la seva comunicació pública des d'un lloc aliè al servei TDX. Tampoc s'autoritza la presentació del seu contingut en una finestra o marc aliè a TDX (framing). Aquesta reserva de drets afecta tant als continguts de la tesi com als seus resums i índexs.

**ADVERTENCIA.** El acceso a los contenidos de esta tesis doctoral y su utilización debe respetar los derechos de la persona autora. Puede ser utilizada para consulta o estudio personal, así como en actividades o materiales de investigación y docencia en los términos establecidos en el art. 32 del Texto Refundido de la Ley de Propiedad Intelectual (RDL 1/1996). Para otros usos se requiere la autorización previa y expresa de la persona autora. En cualquier caso, en la utilización de sus contenidos se deberá indicar de forma clara el nombre y apellidos de la persona autora y el título de la tesis doctoral. No se autoriza su reproducción u otras formas de explotación efectuadas con fines lucrativos ni su comunicación pública desde un sitio ajeno al servicio TDR. Tampoco se autoriza la presentación de su contenido en una ventana o marco ajeno a TDR (framing). Esta reserva de derechos afecta tanto al contenido de la tesis como a sus resúmenes e índices.

**WARNING.** Access to the contents of this doctoral thesis and its use must respect the rights of the author. It can be used for reference or private study, as well as research and learning activities or materials in the terms established by the 32nd article of the Spanish Consolidated Copyright Act (RDL 1/1996). Express and previous authorization of the author is required for any other uses. In any case, when using its content, full name of the author and title of the thesis must be clearly indicated. Reproduction or other forms of for profit use or public communication from outside TDX service is not allowed. Presentation of its content in a window or frame external to TDX (framing) is not authorized either. These rights affect both the content of the thesis and its abstracts and indexes.

Dionysia Tsoutsi

# Inorganic Ions Sensing by surface-enhanced Raman scattering spectroscopy



Doctoral Thesis

Department of Electronic, Electric, and Automatic Engineering  
(DEEEA)



UNIVERSITAT ROVIRA I VIRGILI





Dionysia Tsoutsi

Inorganic Ions Sensing by surface-enhanced  
Raman scattering spectroscopy

DOCTORAL THESIS

Supervised by Prof. Ramón Álvarez-Puebla and  
Dr. Luca Guerrini

Department of Electronic, Electric, and Automatic Engineering  
(DEEEA)



UNIVERSITAT ROVIRA I VIRGILI

Tarragona

2015



## Statement of Supervision



UNIVERSITAT  
ROVIRA I VIRGILI

Department of Electronic, Electric  
and Automatic Engineering (DEEEA)  
Avd. Paisos Catalans 26, Campus Sescelades  
43007, Tarragona, Spain  
Phone: +34 977 558524  
Fax: +34 977 559605

I STATE that the present study, entitled "Inorganic Ions Sensing by surface-enhanced Raman scattering spectroscopy", presented by Dionysia Tsoutsi for the award of the degree of Doctor, has been carried out under my supervision at the Department of Electronic, Electric and Automatic Engineering of this university, and that it fulfils all the requirements to be eligible for the Doctorate Award.

Tarragona (Spain), 29 January 2015

Prof. Ramón Álvarez-Puebla, Doctoral Thesis Supervisor

Dr. Luca Guerrini, Doctoral Thesis Supervisor





*This thesis is dedicated to my beloved parents,*

*Kondylia and Niko.*

*Thank you!*



## **Acknowledgments**

I owe a great many thanks to the many people who guided, helped and supported me during all the stages of this dissertation.

To begin with, I would like to thank my thesis supervisors Prof. Ramón Álvarez-Puebla and Dr. Luca Guerrini for the scientific guidance of this thesis. At this point I would also like to express my special thanks to Prof. Luis M. Liz-Marzan who co-supervised and guided part of this work when I first had the opportunity to start my thesis at the Colloid Chemistry Group of the University of Vigo.

I would like to acknowledge and thank the University Rovira I Virgili for the financial support.

I am particularly grateful for the assistance given by Prof. Roberto Giral and Prof. Lluís F. Marsal. Their help and understanding was crucial for the successful completion of this thesis.

I would also like to express my great appreciation to all of the colleagues that I worked with and inevitably shared, day by day, all our anxieties and moments of joy at the Colloid Chemistry Group of the University of Vigo. To all the people I met and worked with in the University Rovira I Virgili and in the Chemistry Technology Centre of Catalonia (CTQC), I owe a great many thanks for the pleasant working environment, because in such a short period of time they made me feel comfortable.

I am grateful to all of my friends, but to some of them I owe special thanks for all the help and advice concerning this dissertation. Manuel, Munish, Niko and Antonia: thank you!

My sincere thanks to Ángel for the moral support and always being there for me.

Last but not least, I would like to express my deep appreciation and great thanks to my parents, Niko and Kondylia, for their unconditional love, support and caring.



## ***Table of Contents***

<b>Thesis Scope</b>	xv
<b>1. Chapter 1: General Introduction</b>	<b>1</b>
1.1. Raman Spectroscopy	1
1.1.1. Raman Effect	2
1.1.2. Raman Selection Rules	3
1.1.3. Raman Intensities	4
1.2. Surface-enhanced Raman scattering (SERS)	7
1.2.1. Electromagnetic Mechanism (EM)	8
1.2.2. Chemical Transfer Mechanism (CT)	11
1.2.3. Selection Rules	13
1.2.4. Hot Spots	14
1.3. SERS substrates	15
1.3.1. Colloidal silver nanoparticles (AgNPs)	18
1.3.2. AgNPs immobilized on solid substrates	19
1.4. SERS sensing	21
1.5. Bibliography	24
<b>2. Chapter 2: SERS recognition of chloride (Cl<sup>-</sup>)</b>	<b>31</b>
2.1. Introduction	32
2.2. Experimental details	34
2.2.1. Chemicals	34
2.2.2. Silica Bead Functionalization and Synthesis and Adsorption of Gold Seeds (SiO <sub>2</sub> @Au)	34
2.2.3. Silver Growth on the Gold Seeds (SiO <sub>2</sub> @Au@Ag)	35
2.2.4. Synthesis of 2-(2-(6-Methoxyquinoliniumchloride)ethoxy)- thanaminehydrochloride (Amino-MQAE)	35

2.2.5. Material Characterization	36
2.2.6. Theoretical Calculations	36
2.2.7. Fluorescence and Surface-Enhanced Raman Scattering Spectroscopy	36
2.3. Results and discussion	37
2.4. Conclusions	44
2.5. Bibliography	46
<b>3. Chapter 3: Ultratrace level SERS simultaneous determination of Cu(II) and Co(II)</b>	<b>51</b>
3.1. Introduction	52
3.2. Experimental details	
3.2.1. Chemicals	53
3.2.2. Nanoparticle synthesis and functionalization	53
3.2.3. Computational analysis	54
3.2.4. Instrumentation	54
3.3. Results and discussion	54
3.4. Conclusion	62
3.5. Bibliography	64
<b>4. Chapter 4: General Conclusions</b>	<b>69</b>
<b>List of publications</b>	<b>71</b>

## ***List of Abbreviations***

**AgNPs:** Colloidal Silver Nanoparticles

**AuNPs:** Colloidal Gold Nanoparticles

**amino-MQAE:** 2-(2-(6-methoxyquinoliniumchloride)ethoxy) ethanamine hydrochloride

**BT:** Benzenethiol

**CE:** Chemical Enhancement

**CT:** Charge Transfer

**DDA:** Discrete Dipole Approximation

**DFT:** Density Functional Theory

**EF:** Enhancement Factor

**EM:** Electromagnetic Enhancement

**HOMO:** Highest Occupied Molecular Orbital

**IR:** Infrared Spectroscopy

**LbL:** Layer-by-Layer

**LSPR:** Localized Surface Plasmons

**LUMO:** Lowest Unoccupied Molecular Orbital

**MBA:** 4-mercaptobenzoic acid

**MW:** Molecular Weight

**NIR:** Near-Infrared

**PEI:** Polyethylenimine

**PSS:** Polystyrene sulfonate

**RS:** Raman scattering

**SERS:** Surface-enhanced Raman scattering

**SEM:** Scanning Electron Microscopy

**SMSERS:** Single-Molecule SERS

**SPs:** Surface Plasmons

**SSRs:** Surface Selection Rules

**SSRF:** Surface Selection Rules Factor

**TEM:** Transmission Electron Microscopy

**TPY-DTC:** 4-(N-piperaziny)terpyridine dithiocarbamate

**VIS:** Visible

**XPS:** X-Ray Photoelectron Spectroscopy



## ***Thesis Scope***

Since its prediction and discovery, surface-enhanced Raman scattering (SERS) spectroscopy has gradually gained ground among the other established spectroscopic techniques and transformed into one of the most promising and powerful analytical tools nowadays. Predominant to the simple Raman scattering effect which is characterized by extremely low cross-sections with only one in every ten thousand photons being inelastically scattered. Even under resonance conditions, with the excitation of the molecule under study taking place at a wavelength near an electronic transition of the molecule, the Raman scattering can be increased by several orders of magnitude but still not enough, for ultradetection analysis. SERS spectroscopy merges the "fingerprinting" ability arising from the unique Raman signature of every analyte, with ultra high sensitivity, even down to the single molecule regime, due to the enhancement of the electromagnetic field on the surface of a metallic nanoparticle. When the incident light is in resonance with the oscillations of the conduction electrons in a metallic nanoparticle, all the conduction electrons will collectively oscillate in an optical phenomenon known as localized surface plasmon resonance (LSPR). Therefore the LSPR phenomenon is responsible for the strong scattering and absorption of light, typical of a metallic nanoparticle. LSPR also enhances local electric fields on the surface of a nanoparticle at specific domains, known as "hot spots". Every analyte found within these hot spots experiences enormous enhancement in terms of their Raman scattering cross section, and in some cases single molecule detection is possible. All the above described, show the need of particularly precise control at the nanometer scale, which makes SERS a nanoscale phenomenon.

Qualitative and, especially, quantitative determination of inorganic atomic species, such as metal ions, in solution at trace levels are of great interest in a variety of purposes ranging from environmental monitoring to biomedical diagnostics. SERS spectroscopy can successfully compete all the well established analytical techniques in atomic species sensing such as, ion chromatography, atomic absorption (or emission) spectroscopy and ion-sensitive electrodes with its ultralow detection limits, fast and easy sample treatment prior to measurement and non-destructive character. Miniaturized SERS-based sensors permit the interrogation of microsystems such as cells, widening the range of applications of this technique. However, SERS detection of monoatomic species is very challenging due to the fact that they lack vibrational signal. An innovative and careful fabrication of SERS substrates, permits the detection either by

binding to an organic receptor ligand whose SERS signature can be altered by formation of a coordination complex or by using encoded particles with Raman reporters whose SERS intensities are selectively perturbed by complexation of the target ions.

In this research project we exploit all the advantages of SERS spectroscopy as a very sensitive and powerful analytical tool for inorganic ion sensing. In Chapter 1, is presented a brief theoretical background in fundamental theory of the Raman effect and the SERS mechanisms. We also explain the significance and the important role of the SERS substrates. Finally a part of this chapter is dedicated to SERS sensing methods and advances.

In Chapter 2 we report a SERS-based chloride sensing ultradetection and quantification method. We monitor the vibrational changes introduced upon interaction with a Cl-sensitive probe supported onto a nanostructured silver-coated silica microbead. In this chapter we describe the important role that the engineered particles play, in the detection. The presented results contribute toward the fabrication of microsensors for fast ultradetection and quantification of representative atomic ions of biological importance.

Chapter 3 deals with the simultaneous and independent SERS sensing of two environmental metallic pollutants, Cu(II) and Co(II). The terpyridine (TPY) derivative is used as the sensitive Raman probe due to the high affinity toward the transition metal ions. Alterations in the SERS vibrational pattern of the dithiocarbamate anchored terpyridine (TPY-DTC) in the presence of the metal ions were directly described as a function of the metal ion nature and concentration. Subsequently, we demonstrated the simultaneous ultradetection of Co(II) in the presence of high Cu(II) concentration.

Finally, Chapter 4 is dedicated to the most relevant and global conclusions derived from this work.

## *Chapter 1: Introduction*

---

### 1.1 Raman Spectroscopy

In 1928 the Indian scientist Sir Chandrasekhara Venkata Raman, together with K. S. Krishnan and independently by Grigory Landsberg and Leonid Mandelstam in the former Soviet Union,<sup>1</sup> were the first to experimentally demonstrate the phenomenon named after him as Raman scattering (RS) or Raman effect which led him a couple of years later to be awarded with the Nobel Prize in physics (1930) for his work on the scattering of light and the discovery of the Raman effect.<sup>2</sup> It must be recalled though, that the theoretical principle of this effect was predicted by the Austrian scientist Adolf Smekal in 1923.<sup>3</sup> Raman spectroscopy is based on the Raman effect which lies in the inelastic light scattering by any particular substance upon illumination. In the original experiment a simple hardware setup, consisted of sunlight as the light source focused onto the sample, passing through a telescope.<sup>4</sup> The sample could be either a liquid or its dust-free vapor.

At first, the phenomenon was measured on a number of different common liquids with the observer's eye to be the proof of the existence of a modified scattered radiation. However, the Raman scattering is a very weak effect. Only one in ten millions of the scattered light particles, or photons, actually exhibits a change in wavelength. Because of this, advances in Raman spectroscopy were delayed for several decades, until the discovery of intense light sources to amplify the effect and consequently the observed scattered light. The laser as an intense and efficient light source from one hand, along with the development of more effective detection systems on the other hand, brought breakthrough changes later on, in the field of Raman spectroscopy.

### 1.1.1. Raman effect

Absorption or scattering are among the major phenomena that may occur when light interacts with matter. Absorption occurs when the energy of the incident photon, which the light is composed of, corresponds to the energy gap between the ground state of an atom or a molecule and an excited state. The photon may be absorbed and the molecule will be promoted to an excited state of higher energy. In the case when the energy of the incident photon does not correspond to a specific energy level of an excited state of an atom or a molecule upon illumination, scattering may occur. The predominant part of the photons are elastically scattered in a process called Rayleigh scattering. During this process the scattered photons have the same frequency as the incident photons ( $\nu_0$ ). A very small fraction of the scattered light, one in a  $10^6$ - $10^8$  photons, undergoes inelastic scattering in the process known as Raman scattering, resulting in a scattered photon with different frequency than the incident photon. In this case, the energy of the scattered photon is different from that of the incident photon by one vibrational unit. For example if the energy of incident photon is  $h\nu_0$ , the difference between the two energy states ( $V_0$  and  $V_1$ ) is  $h\Delta\nu$ .

The Raman scattering effect comes from the fact that the light interacts with the molecule and distorts, polarizes, the cloud of electrons surrounding the nuclei to form a short-lived state known as "virtual state". This state is not a stable stage and the photon is re-radiated. This occurs when the light and the electrons interact and the nuclei begin to move at the same time. Since the nuclei are much heavier than the electrons, there is a change in energy of the molecule. Transfer of energy will occur either from the incident photon to the atom or molecule or from the atom or molecule to the scattered photon. Depending on whether the process starts with a molecule in the ground state or from an atom in a vibrationally excited state, the scattering process may be classified as Stokes or anti-Stokes scattering. Stokes scattering occurs from the ground vibrational state ( $V_0$ ) to an excited vibrational state ( $V_1$ ) due to the energy absorption by the molecules ( $h\Delta\nu$ ). However, some molecules due to thermal energy may be already in an excited state ( $V_1$ ) as shown in figure 1.1. Therefore anti-Stokes scattering occurs from the excited state ( $V_1$ ) to the ground state ( $V_0$ ) a process that involves energy transfer to the scattered photon ( $h\Delta\nu$ ). The relative intensities of these two processes depend on the population of the various states of the molecules. The fact that the majority of the molecules are in room temperature, very small number of atoms are expected to be found to an excited state.

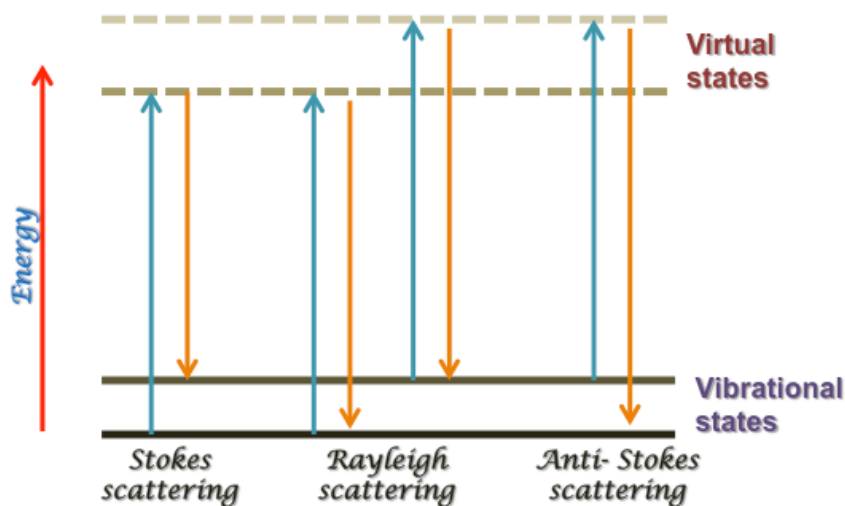


**Figure 1.1.** Schematic representation of the Rayleigh and Raman scattering

### 1.1.2. Raman selection rules

The infrared (IR) spectroscopy and the Raman spectroscopy are the two types of spectroscopy that involve vibrational transitions. The fundamental vibrational transitions can be studied by both IR and Raman spectroscopy because they have different selection rules. Whether a transition is allowed or not, is defined by the selection rules. For Raman scattering the fundamental selection rule is the one that occurs from the change in polarizability in a molecule. The polarizability is a molecular property and measures the deformability of a bond under the influence of an external electric field, inducing a temporary dipole. Symmetric vibrations will give the most intense Raman scattering (Raman-active). Unlike to Raman spectroscopy, in IR spectroscopy, an asymmetric vibration (IR-active) will be more intense when a net change in the permanent dipole moment occurs during the vibrations.

In figure 1.2., the symmetric stretch in carbon dioxide is not IR-active because no net change occurs in the dipole moment. The asymmetric stretch is IR-active due to a change in dipole moment.

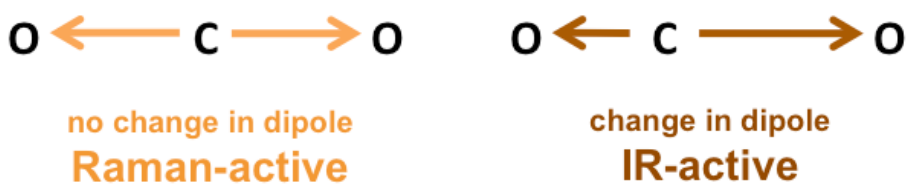


**Figure 1.2.** IR and Raman active vibrations of carbon dioxide.

The symmetric stretch in carbon dioxide is Raman-active due to the change of the polarizability of the molecule. Figure 1.3. illustrates the different shapes of the electron cloud which can be found during the equilibrium, the extended and compressed symmetric motions.

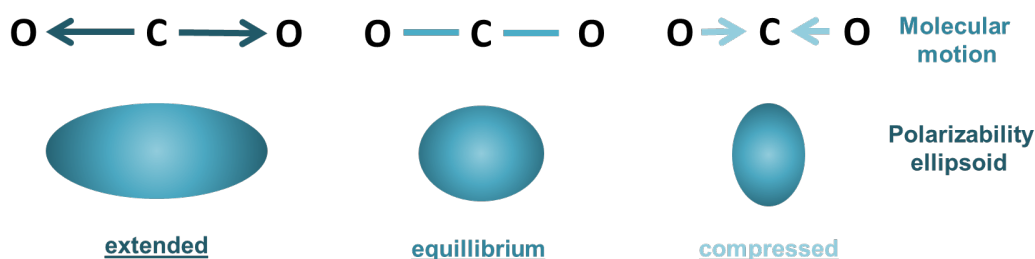


**Figure 1.3.** Changes of the polarizability of the molecule of carbon dioxide.

### 1.1.3. Raman Intensities

The Raman effect, from a classical wave interpretation, considers light as an electromagnetic radiation which contains an oscillating electric field that interacts with an atom or a molecule through its polarizability. The theory of the polarizability was developed by a Czech scientist, George Placzek in 1934, and can be used to justify many of the important features of Raman band intensities.

From the point of electrostatics, the electric field,  $\mathbf{E}$ , is associated with the electromagnetic radiation which induces a dipole moment,  $\boldsymbol{\mu}$ , given by the following equation:

$$\boldsymbol{\mu} = \alpha \mathbf{E} \quad \text{Equation 1.1}$$

where  $\alpha$ , is the polarizability of the molecule. The electric field vector  $\mathbf{E}$  is given by:

$$E = E_0 \cos 2\pi \nu_0 t \quad \text{Equation 1.2}$$

where  $E_0$  is the amplitude and  $t$  is the time, is proportional to the field as follows:

$$\mu = aE_0 \cos 2\pi \nu_0 t \quad \text{Equation 1.3}$$

The polarizability, which is a tensor quantity, indicates the ability of the electrons of the electron cloud to be polarized when the molecule is illuminated by light. If the molecule itself is vibrating at a frequency  $\nu$  corresponding to its normal mode, then for small amplitudes of vibration,  $a$  is a linear function of  $Q_0$  as follows:

$$a = a_0 + (\partial a / \partial Q)_0 Q \quad \text{Equation 1.4}$$

where  $a_0$  is the polarizability at the equilibrium position, and the  $(\partial a / \partial Q)_0$  is the rate of change of  $a$  with respect to the change in a normal coordinate  $Q$  evaluated at equilibrium position. The normal coordinate of the nuclear displacement  $Q$  is given by:

$$Q = Q_0 \cos 2\pi \nu t \quad \text{Equation 1.5}$$

where  $Q_0$  is the vibrational amplitude. By combining the above equations starting from the equation 1.3, one can obtain the following:

$$\begin{aligned} \mu &= aE_0 \cos 2\pi \nu_0 t \\ \mu &= a_0 E_0 \cos 2\pi \nu_0 t + (\partial a / \partial Q)_0 Q_0 E_0 \cos 2\pi \nu_0 t \cos 2\pi \nu t \quad \text{Equation 1.6} \end{aligned}$$

$$\begin{aligned} \mu &= a_0 E_0 \cos 2\pi \nu_0 t \\ &\quad + \frac{1}{2} (\partial a / \partial Q)_0 Q_0 E_0 \{ \cos[2\pi(\nu_0 + \nu)t] + [\cos 2\pi(\nu_0 - \nu)t] \} \end{aligned}$$

The Rayleigh scattering of frequency  $\nu_0$  is given by the first term while the Raman scattering of frequencies  $(\nu_0 - \nu)$  and  $(\nu_0 + \nu)$  is described by the second term. The increase in frequency,  $(\nu_0 + \nu)$ , is known as an Anti-Stokes shift and the

decrease in frequency,  $(\nu_0 - \nu)$ , is known as a Stokes shift. These shifts correspond to modulations by the vibrational frequency of the bond.

The equation 1.6 shows the conditions that should be met in order to achieve an intense Raman intensity. Molecules with larger polarizability and that experience a strong electric field play an important role. In the case where a vibration does not greatly change the polarizability, then the polarizability derivative will almost be zero, therefore the intensity of the Raman band will be low. The intensity of a Raman band  $I_R$  is proportional to the square of the induced dipole moment,  $\mu$ , which is proportional to the square of the polarizability derivative as follows:

$$I_R \propto (\partial\alpha/\partial Q)_0^2 \quad \text{Equation 1.7}$$

when  $(\partial\alpha/\partial Q)_0 = 0$ , the vibration is not a Raman active mode according to the Raman selection rule because the polarizability does not change during the vibration.

For several decades unfortunately, Raman spectroscopy was not among the most popular analytical techniques. Fundamental factor for this is that the Raman effect itself is a very weak process which leads to poor sensitivity. Raman cross-section,  $\sigma$  ( $\text{m}^2$ ), though empirically determined, was introduced in order to quantify the efficiency of the process.<sup>5</sup> From the experimental point of view the beam is characterized by its power,  $P$  (in W), which is proportional to the number of incident photons per unit area and the number of photons that can interact with the molecule in a certain way, which is proportional to the power density  $S$  (in  $\text{W m}^{-2}$ ) at the molecule position. The Raman cross-section is described by the following equation<sup>6</sup>:

$$P = \sigma S \quad \text{Equation 1.8}$$

Raman scattering is a second-order process and the differential Raman cross-section ( $d\sigma/d\Omega$ ) of only  $10^{-31}$ - $10^{-26}$   $\text{cm}^2$  can be confirmed when compared, for example, with the  $10^{-16}$   $\text{cm}^2$  per molecule in a typical fluorescence cross-section. Additionally, fluorescence is a competitive effect which normally overlaps a weak Raman signal. However, the advances in instrument technology have simplified the equipment and reduced the problems substantially. The discovery of the surface-



enhanced Raman scattering effect, decades later, along with the advances in metallic nanocrystal synthesis and instrument technology improvements, brought a great impact in the applications of the Raman spectroscopy as a potent analytical tool.

## 1.2. Surface-enhanced Raman scattering

Surface-enhanced Raman scattering (SERS) is the remarkable amplification of the Raman signal exploiting the interaction between light, molecules and metal nanostructured surfaces, by several orders of magnitude until the observation of single-molecule SERS (SMSERS)<sup>7,8,9</sup> with enhancement factors  $>10^{13}$ . First observation of the SERS effect was made by Fleischmann, Hendra, and McQuillan in 1974.<sup>10,11</sup> They reported enhancement of the Raman signal of pyridine on a silver electrode when roughened by means of successive oxidation-reduction cycles. The first interpretation in the original paper, Fleischmann et al. claimed that the observed enhancement of the Raman signal of pyridine is a result of the increased surface area caused by the roughening of the silver electrodes. A couple of years later two independent research groups, Jeanmarie and Van Duyne<sup>12</sup> and Albrecht and Creighton<sup>13</sup> claimed that the high surface area is not responsible for the observed Raman enhancement and the concept of enhancement mechanisms is reported. The enhancement is related to the electromagnetic interaction of light and metallic nanoparticles, which causes strong electromagnetic fields, localized around the nanoparticles through plasmon resonances. Molecules in close vicinity or attached directly to the metallic nanostructured surfaces can be affected by the strong plasmonic field, therefore an amplification of the Raman signals of molecules occurs. 30 years after its discovery, several enhancement mechanisms have been proposed in order to explain the SERS effect. Only two mechanisms are broadly accepted, the electromagnetic (EM) mechanism and the chemical enhancement (CE) mechanism. The latter depends on the chemical interaction between the probe molecules and the metallic surface and contributes approximately to 2-3 orders of magnitude.<sup>14</sup> The EM mechanism is recognized as more essential for SERS and is based on the collective oscillation of free electron density, generating localized surface plasmons (LSPs) and can contribute ten or more orders of magnitude enhancement.<sup>15</sup>

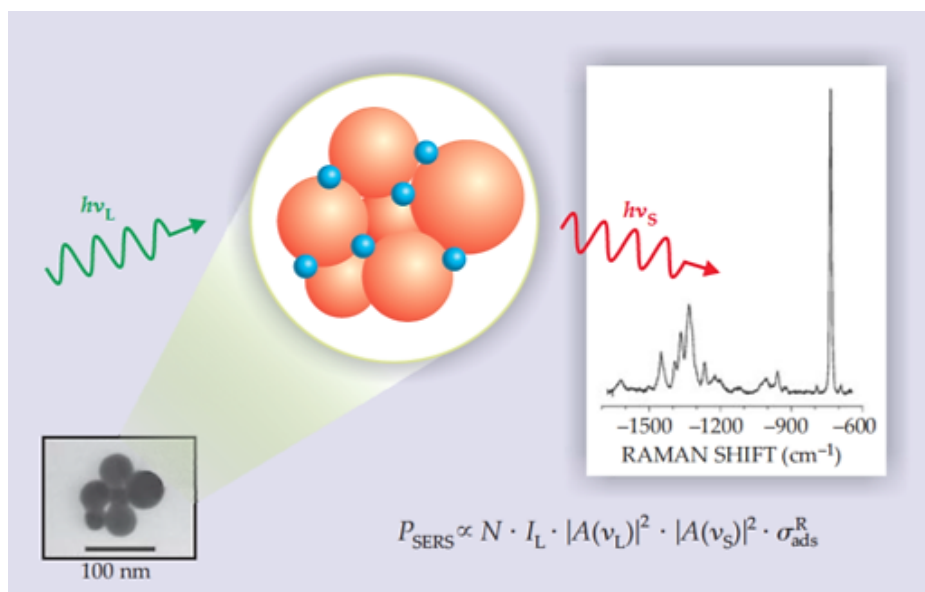


**Figure 1.4.** Molecules (blue spheres) are adsorbed onto the surface of metal nanostructures (orange spheres). The SERS spectrum reveals molecular-vibration energies based on the frequency shift between the incident (green line) and the scattered light (red line).

### 1.2.1. Electromagnetic mechanism

The majority of the overall SERS enhancements are due to the EM enhancement mechanism as a result of the localized surface plasmon resonance excitation, present on the noble metal surfaces.<sup>16,17,18,19,20,21</sup> In order to understand the EM enhancement mechanism, it is important to make an insight in the localized surface plasmon resonances (LSPRs). This phenomenon, when confined to a particle of a size comparable to the wavelength of the light can be attributed to the collective oscillation of the particle's free electrons. The LSPR is directly associated with the sharp spectral absorption and scattering peaks of noble metal nanostructures, along with strong electromagnetic near-field enhancements at the particle's surface which exponentially decay away from it.<sup>22</sup> For instance, if the morphology of a nanostructure is spherical and its size is small enough compared to the wavelength of incident radiation, the collective oscillation of the free electrons is dipolar in nature as is illustrated in the following figure 1.5.<sup>23</sup>

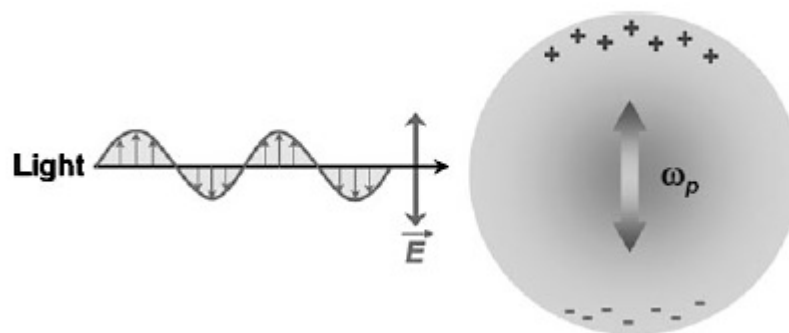


**Figure 1.5.** Illustration of plasmon oscillation for a metal nanosphere. Interaction of the electromagnetic wave with a metal causes the free electrons to coherently oscillate at the plasmon frequency ( $\omega_p$ ) against the immobile positive-ion lattice.

Consequently, the adequacy of a material, usually a metal, for SERS use depends strongly from the metal nature itself. The dielectric function of a metal is metal-dependent and indicative of how much absorbs or scatters light and is divided in two parts.<sup>22</sup> The real part is related to the scattering efficiency and the imaginary part is associated to the absorption efficiency. A negative real part and a small imaginary part of the dielectric function of a metal is the convention for SERS suitability. Noble metals such as Ag, Au, Cu and the alkaline are among the materials that best fulfill the above condition for SERS use. Thus, in silver the real part of its dielectric function is larger than in gold which is translated in better scattering efficiency making silver by far the most important metal in SERS spectroscopy.

Next, the *local field* and *radiation* enhancement factors and the common  $\mathbf{E}^4$  approximation to the single-molecule EF (SMEF), are introduced.

- *Local field enhancement*

The electromagnetic field is strongly affected upon interaction with metallic surfaces and especially under certain conditions as when the excitation wavelength is close to the LSPR. Therefore at the molecule position, the electric field  $\mathbf{E}_{\text{Loc}}$  can differ considerably both in magnitude and orientation, to the incident field  $\mathbf{E}_{\text{Inc}}$ . The local field  $\mathbf{E}_{\text{Loc}}$  is the electric field felt by the molecule. It depends on the excitation wavelength and polarization, and can be dramatically affected by the position. The magnitude  $|\mathbf{E}_{\text{Loc}}|$  on the metallic surface can be much higher than  $|\mathbf{E}_{\text{Inc}}|$  due to specific positions on the surface, the so-called 'hot-spots'. The  $\mathbf{E}_{\text{Loc}}$  induces a Raman dipole given as:

$$p_R = \alpha_R E_{Loc}(\omega_L) \quad \text{Equation 1.9}$$

whose magnitude is enhanced by a factor  $|E_{Loc}(\omega_L)| / |E_{Inc}|$ . In such a dipole the energy radiated in free-space is proportional to  $|p_R|^2$  and can be enhanced by a factor:

$$M_{Loc}(\omega_L) = \frac{|E_{Loc}(\omega_L)|^2}{|E_{Inc}|^2} \quad \text{Equation 1.10}$$

$M_{Loc}(\omega_L)$  is the local electric field enhancement factor and characterizes the enhancement of the electric field intensity, but ignores any changes in the electric field polarization.

- *Radiation enhancement*

Under SERS conditions, the Raman dipole radiates in presence of metallic objects, unlike in free-space. The close proximity to the metal alters the dipole radiation in the same manner as the incident electric field is modified. The total power radiated by the dipole,  $P_{rad}$  can be either quenched or enhanced relatively to that in free space,  $P_0$ , depending on the relative dielectric function  $\epsilon(r)$  of the object, its geometry, and the dipole position, orientation and its emission frequency,  $(\omega_R)$ .

For objects having negative real dielectric function, the radiated power is strongly enhanced and is due to coupling to the LSPR of metallic objects.<sup>5</sup> The radiation enhancement factor is given by:

$$M_{Rad} = P_{Rad}/P_0 \quad \text{Equation 1.11}$$

- *E<sup>4</sup> approximation*

The E<sup>4</sup> approximation is considered to be a common model to explain the EM enhancement in SERS and is given by the following equation:

$$EF \approx M_{Loc}(\omega_L)M_{Rad}^d(\omega_R) \quad \text{Equation 1.12}$$

where  $M_{Loc}(\omega_L)$  can be calculated by solving the electromagnetic problem under specific external excitation conditions with an incident field,  $\mathbf{E}$ , which yields local field everywhere.

Calculating the  $M_{Rad}^d$  is a more difficult task and it is necessary to solve the electromagnetic problem of dipolar emission, instead of external excitation, which itself is very complicated. For simplicity, it is generally assumed that the local electric field enhancements and radiation enhancements are approximately equal,  $M_{Rad}^d(\omega) \approx M_{Loc}(\omega)$ . The enhancement factor can then be expressed as:

$$EF \approx M_{Loc}(\omega_L)M_{Loc}(\omega_R) \approx \frac{|E_{Loc}(\omega_L)|^2}{|E_{Inc}|^2} \frac{|E_{Loc}(\omega_R)|^2}{|E_{Inc}|^2} \quad \text{Equation 1.13}$$

which at zero-Stokes shift  $\omega_L \approx \omega_R$  yields the  $E^4$  approximation expressed as:

$$EF(\omega_L) \approx \frac{|E_{Loc}(\omega_L)|^4}{|E_{Inc}|^4} \quad \text{Equation 1.14}$$

The above equation is the most important expression in SERS. By this approximation at specific positions on the substrate one can obtain the right order of magnitude for the single-molecule EF (SMEF), while average EF can also be derived by surface averaging. However, these approximations do not stand for polarization effects or surface selection rules in SERS.

### 1.2.2. Chemical transfer mechanism

The other major contribution to SERS EF factor is the chemical enhancement, also referred as charge transfer (CT) and short-range effect. This process involves the formation of a bond between the analyte and the metal surface. In comparison to EM enhancement, aspects of chemical enhancement contribution are less studied.<sup>24,25</sup> This mechanism is site-specific and analyte-dependent and is generally thought to

contribute by only a factor of  $10-10^2$  compared to the EM enhancement. One principle is that the molecule should be directly adsorbed to the roughened surface to experience the chemical enhancement, thus, any variation to the experimental parameter will affect both mechanisms, making the separation of two effects very difficult.<sup>26</sup> The profound understanding of the chemical mechanism process is of great importance due to the fact that the observed SERS spectra behold information about the probe molecule and its environment.

The first evidence of the charge-transfer effect were observed when the molecules of CO and N<sub>2</sub> were found to differ by a factor of 200 in their SERS intensities under the same experimental conditions while the EM enhancement should be a nonselective amplifier for Raman scattering by all molecules adsorbed on a plasmonic surface. Both molecules have almost the same polarizabilities but differ substantially in the orientation. The latter could explain the difference observed in the enhancement factor. Additionally another evidence of the CM is the potential-dependent electrochemical experiments where the potential is scanned at a standard laser frequency, or the laser frequency is scanned at a standard potential and broad resonances are observed.

This can be explained by the resonance Raman mechanism in which either the electronic states of the molecule adsorbed, upon interaction with the metallic surface are broadened and shifted, or new electronic states arise, acting as resonant intermediate states in Raman scattering. Figure 1.6. shows a typical energy level diagram for a molecule adsorbed on a metal. The highest occupied molecular orbital (HOMO) and lowest unoccupied molecular orbital (LUMO) of the molecule are symmetric relative to the Fermi level of the metal. The three possible CT processes are also presented involving molecular and metallic states (b, c) and only molecular states (a). Factors as the adsorption site, the geometry of bonding and the energy levels of the molecules are very important and this mechanism can provide useful information on the interactions between metals and molecules chemically bonded. In general the SERS CT mechanism is considered to contribute the EF on the order of up to  $10^3$ .<sup>27</sup>

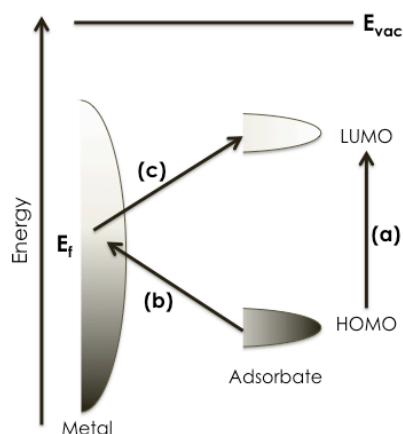


**Figure 1.6.** Schematic diagram of the three-step process of the charge transfer mechanism in SERS

### 1.2.3. Selection rules

Surface selection rules factor (SSRF) plays a key role in terms of the polarization effects in SERS and bring an insight on molecular absorption or molecular orientation effects in SERS. It is generally admitted that this is not an easy task but rather a complicated factor because it involves the polarization of the local field for both the real and 'virtual' problems and for these reasons in most SERS theoretical or experimental is ignored.

Originally this effect was studied for molecules chemisorbed on planar metallic surfaces, for which analytic EM solutions exist. The prediction of the changes in the relative intensities of Raman modes with different Raman tensor symmetries for a fixed molecular adsorption on the surface are commonly called surface selection rules (SSRs).<sup>28</sup> Only recently this study was extended to more realistic SERS substrates, such as those containing hot-spots.<sup>29,30</sup> Planar surfaces possess the advantage of simplicity but the SERS EF on them are almost negligible for any real application of the effect. All the above mentioned effects are contained in the surface selection rules factor  $T$ . The  $T$  depends on the local field polarization at the molecule position for both the real excitation  $e_L = e_{Loc}(\omega_L)$  and the 'virtual'  $e_R = e_{Loc}^{PW-P}(\omega_R)$ .

The  $T$  must remain positive, and for an appropriate combination of  $e_L$  and  $e_R$  may equal to zero. The maximum value of  $T$ , for a given tensor  $\hat{a}_N$ , is obtained for the largest eigenvalue of  $\hat{a}_N$ . When considering all possible Raman tensors, one can show

that the largest possible value for  $\mathbf{T}$  is being obtained for a uni-axial tensor when both  $e_L$  and  $e_R$  are along the tensor axis, given by the following inequality.<sup>31</sup>

$$0 \leq T(\hat{a}_N, e_L, e_R) \leq 15/4$$

which justifies that  $\mathbf{T}$  in most cases, is a secondary effect on the overall magnitude of the SMEF.

All of the above, when applied for a fixed molecule orientation can be also applied in the case of orientation averaging. The orientation-averaged SSRF SSRF  $\langle T(\hat{a}_N, e_L, e_R) \rangle$  is given by:

$$\langle T(\hat{a}_N, e_L, e_R) \rangle = \frac{\rho + (1 - \rho)|e_L \cdot e_R|^2}{1 + \rho}$$

$\rho$ : is the non-SERS depolarization ratio where the exact value therefore depends on the relative orientation of the  $e_L$  and  $e_R$  but remains in the range:

$$\frac{\rho}{1 + \rho} \leq \langle T(\hat{a}_N, e_L, e_R) \rangle = \frac{1}{1 + \rho}$$

for  $e_L = e_R$  the maximum is obtained and is valid that  $0 \leq \langle \mathbf{T} \rangle \leq 1$  independently of the specific type of Raman tensor.

#### 1.2.4. Hot Spots

An additional EF arises from the interaction of two or more neighbouring nanoobjects. Maximum SERS EF typically occurs at some specific regions on the substrate's surface where the LSPRs are coupled between individual nanostructures resulting in significantly higher electromagnetic field and molecules adsorbed on these points can profit from it.<sup>32,33</sup> The maximum SERS EF may be of the order of  $\sim 10^6$  on a spherical nanoparticle and under certain conditions can be as high as  $\sim 10^{10}$ - $10^{11}$ . As an example of such cases is the apex of a metallic tip or a nanometer gap between two nanoparticles.



The theoretical approach was developed by Shalaev et al and predicts extremely large electromagnetic field enhancement on fractal surfaces.<sup>34,35,36</sup> It was experimentally determined that the strong enhancement occurs in these specific regions, hot spots, by combining the discrete dipole approximation (DDA) method and the fractal features from the aggregated colloids or rough surfaces.<sup>37,38</sup> It is in these special regions that the resonance of the electromagnetic radiation is concentrated. The locations of the hot areas depend strongly on the geometry of the fractal, the excitation wavelength and the polarization of the incident laser. In addition, it has been demonstrated that the same area could be a hot spot or a cold zone depending on the excitation wavelength used.

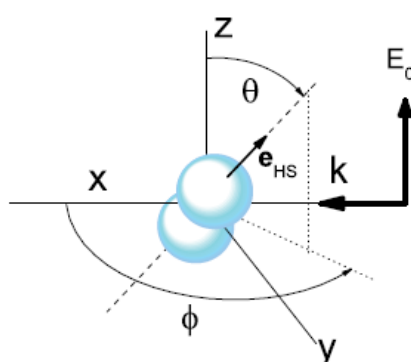


**Figure 1.7.** A schematic configuration for the hot spot problem. The incoming wave is incident along the  $x$ -axis with polarization along  $z$ , and the signal is analyzed in the backscattered direction with polarization either parallel  $\parallel$  ( $z$ ) or perpendicular  $\perp$  ( $y$ ) to the incoming polarization. The main axis joining the two particles, which defines the direction of the main axis of the hot spot,  $\mathbf{e}_{\text{HS}}$  is defined by angles  $\theta$  (co-latitude) and  $\phi$  (longitude) in spherical coordinates

In the above figure we can see a geometrical scheme of a hot spot. The excitation beam is considered to be incident along  $x$  and perpendicular to the dimer axis along  $z$  and we consider excitation occurring only with incident polarization along the dimer axis, for which maximum coupling to the main LSP resonance is obtained.<sup>39</sup>

### 1.3. SERS substrates

The success condition for the SERS studies is highly dependent on the interaction between the absorbed probe molecule and the surface of the plasmonic nanostructure. The synthesis of metal nanoparticles is an expanding research area due

to the potential applications for the development of novel technologies. The most used substrates in SERS are made mostly of silver (Ag), gold (Au), which are good candidates due to their stability and biocompatibility of the Au, and much less of copper (Cu) due to its high reactivity. Most Raman measurements occur in the visible and near infrared wavelength range where all the three metals mentioned above hold LSPRs.<sup>40</sup>

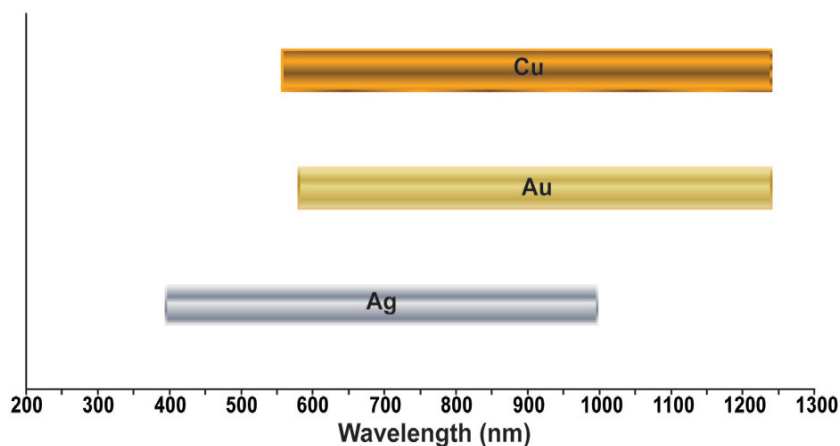


**Figure 1.8.** Approximate wavelength ranges where Ag, Au, and Cu have been well-characterized and are established to support SERS

Nevertheless SERS experiments have been performed in other metals like rhodium (Rh),<sup>41</sup> platinum (Pt),<sup>42</sup> ruthenium (Ru)<sup>43</sup>, and aluminium (Al).<sup>44</sup> Novel materials such as graphene,<sup>45,46</sup> semiconductors such as TiO<sub>2</sub>,<sup>47</sup> and quantum dots (QDs)<sup>48,49</sup> have recently been reported to show SERS, although they do not fit traditional definitions of SERS substrates.

Many factors need to be considered when classifying a material as a reliable and highly enhancing SERS substrate. Generally SERS-active substrates can be roughly classified into following three categories:

- Metallic nanoparticles in suspension, such as colloidal solutions.
- 'Planar' metallic structures, such as arrays of metallic nano-particles supported on a planar substrate (glass, silicon, metals, etc).
- Metallic electrodes.

Metal colloids in suspension or immobilized, predominantly made of Ag or Au, represent one of the simplest and easiest route to SERS because the colloidal

synthesis is relatively easy, but still challenging, in the laboratory. Since Faraday's pioneering work, the main aim has been the control over the synthetic parameters of colloidal metal nanoparticles.<sup>50</sup> Plenty of synthetic interest on the field resulted in the development of a high number of methods for the preparation of colloidal nanostructures with SERS activity which still remain nowadays.

The two most popular approaches are the top-down and bottom-up nanofabrication.<sup>51</sup> A typical top down method for example involves the mechanical grinding of bulk metals and subsequent stabilization of the resulting nanoscaled metal particles by the addition of colloidal protecting agents. On the other hand, the bottom up methods of wet chemical nanoparticle synthesis rely on the chemical reduction of metal salts, electrochemical pathways, or controlled decomposition of metastable organometallic compounds. A large variety of polymers and surfactants are used to control the growth of the primarily formed nanoclusters and to prevent them from aggregating.<sup>52</sup>

The most popular method used for the preparation of metal nanoparticles in suspension for SERS is chemical reduction which is generally performed by using a metal salt and a chemical reducing agent to produce colloidal suspensions containing nanoparticles with variable sizes, depending on the method of production. Suitable for SERS experiments, are sizes that span from 10 to 80nm and will therefore support different plasmon resonances, depending on the size, shape and dielectric constant of the metal. The size and shape parameters can be partially controlled by appropriate choice of preparation methods. The most important parameters in this regard are the nature of the metal, the reducing agent, the temperature, the stabilizing agents and the metal ion concentration.<sup>53</sup>

The first published work using metal colloids in order to achieve the SERS spectrum of pyridine was in 1979 by the Creighton et al. group.<sup>54</sup> The synthesis included silver colloids by the reduction of  $\text{AgNO}_3$  with  $\text{Na}(\text{BH}_4)$  and gold colloids by the reduction of  $\text{K}(\text{AuCl}_4)$  with  $\text{Na}(\text{BH}_4)$ . One year later, the Kerker et al. group reported SERS from citrate reduced silver colloids.<sup>55</sup> Since then, metal colloids have become one of the classical SERS substrates and they provide one of the most reliable SERS methodologies to obtain average enhancement values.

### 1.3.1. Colloidal silver nanoparticles (AgNPs)

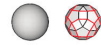










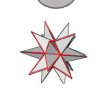

Possibly Ag is the most important material in plasmonics. This increasingly rapid interest is due to its promising applications in the fields of plasmonics. Since SERS is derived from the LSPRs in nanostructured metals, Ag outperforms the other due to its higher extinction coefficients, sharper extinction bands, higher ratio of scattering to absorption, and extremely high field enhancements. Silver is able to support strong surface plasmons, SPs, in the visible (vis) and near-infrared (NIR) regions of the spectrum by tuning its size and shape.<sup>56</sup>

Nowadays, advances in synthetic methods allow the generation of Ag nanostructures with varied morphological properties which overcome the difficulties of the precise control of the Ag due to its lower chemical stability when compared to gold.<sup>57,58,59</sup> In the table 1 are presented briefly some of the synthetic methods used to generate certain morphologies.

Herein will be presented briefly the most common and simple approach that primarily uses chemical reduction to generate elemental Ag from a precursor salt and therefore generate Ag nanostructures. In past studies, silver nitrate, AgNO<sub>3</sub>, was the most commonly used precursor and typically used as chemical reducing agents are sodium borohydride, alcohols, and sodium citrate which reduce Ag<sup>+</sup> ions to Ag atoms, which grow into small clusters and eventually nanostructure.<sup>60,61,62</sup> The polymers and the surfactants apart from stabilizing the particles during and after formation, they also play the role to direct particle growth to the desired shapes. Nowadays AgNPs can even be synthesized and stabilized by peptides, proteins, DNA and chemical/biological polymers.

In 1982, was first reported the synthesis of Ag colloids by the chemical reduction of AgNO<sub>3</sub> with citrate as the reducing agent in aqueous solution by Lee and Miesel.<sup>63</sup> This approach still remains a classic synthesis approach to quickly produce Ag colloids. In a typical synthesis, Ag nanoparticles are obtained by adding a fix concentration of aqueous sodium citrate into a boiling aqueous solution of AgNO<sub>3</sub> and wait for 1 h before letting the system to cool down. Unfortunately, the Ag sol synthesized using this simple method tends to contain a large diversity of sizes ranging from a few nanometers to some hundreds and the shape diversity of shapes (polyhedrons, plates, spheres, wires) is also uncontrollable. This material is although useful for reliable SERS studies due to its high efficiency and easy surface modification by interchanging easily the adsorbed citrate with the molecule under study.

**Table 1.** Summary of the Shapes, LSPR Absorption Peaks, Demonstrated Applications, and Methods for Synthesis of AgNPs

Shape	Illustration	LSPR <sup>a</sup>	Applications <sup>b</sup>	Method of Synthesis
Sphere and quasi-sphere		320 - 450	SERS; LSPR sensing; assembly	Polyol process (single-crystal); Citrate reduction (quasi-sphere)
Cube and truncated cube		400 - 480	SERS; LSPR sensing; assembly	Polyol process; Seed-mediated growth
Tetrahedron and truncated tetrahedron		350 - 450	SERS	Polyol process; Light-mediated Growth
Octahedron and truncated octahedron		400 - 500	Assembly	Polyol process; seed-mediated growth; light-mediated growth
Bar		350 - 900	SERS	Polyol process
Spheroid		350 - 900	SERS	Polyol process
Right bipyramid		500 - 700	-	Polyol process
Beam		-	Electron transport	Polyol process
Decahedron		350 - 450	-	Seed-mediated growth; light-mediated growth; citrate reduction
Wire and rod		380 - 460	Wave guiding; electronics; SERS; assembly	Seed-mediated growth
Polygonal plates and disc		350 - 1000	SERS; LSPR sensing	Light-mediated growth; polyol process
Branched structures		400 - 1100	SERS	Seed-mediated growth
Hollow structures		380 - 800	SERS; LSPR sensing	Template-directed growth

<sup>a</sup> The main absorption peak (nm). <sup>b</sup> Assembly means the nanostructure has been assembled into larger structures for plasmonic applications or studies.

### 1.3.2. AgNPs immobilized on solid substrate

The easiest route to create nanostructured thin films as SERS substrate is to immobilize the nanoparticles simply by drying silver sols onto a macroscopic substrate (glass slides, silicon). The drying method on the surface of the substrate can happen either by a simple drop-casting or through dipping of the substrate at a controlled speed. Straightforward drop-casting typically results in fractal-like arrangement of the particles with very high EM enhancement due to the large number of hot-spots, but with large spatial inhomogeneities and non-uniformity in the coverage of the surface. On the other hand dipping of substrates at a controlled speed has as a result a more uniform distribution of the particles providing similar quality of hot-spots, suitable for specific SERS studies.

Another strategy often used to controllably deposit AgNPs on a solid substrate is the layer-by-layer (LbL) self-assembly, according to which, the substrate's surface is modified in an appropriate way that will facilitate the adsorption of the silver colloids. Self-assembly is a process where pre-existing components spontaneously organize driven by interacting forces such as the electrostatic attraction between subsequent layers of oppositely charged polyelectrolytes on a glass slide as illustrated in figure 1.9<sup>64,65,66,67</sup> By having control over the experimental parameters one can achieve different types of particle deposition on the substrate or in other words, different type of interaction between the immobilized particles therefore different plasmonic response.

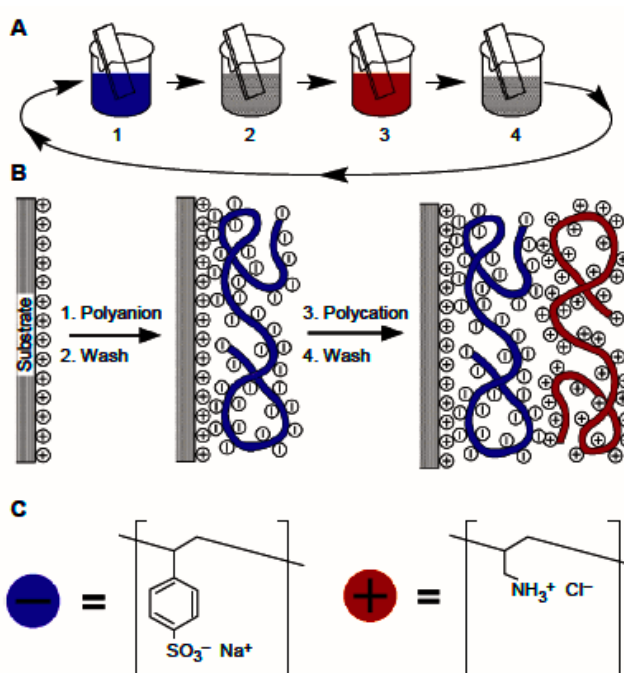


**Figure 1.9.** **A.** Schematic of the film deposition process using slides and beakers. Steps 1 and 3 represent the adsorption of a polyanion and polycation, respectively, and steps 2 and 4 are washing steps. The four steps are the basic buildup sequence for the simplest film architecture,  $(A/B)_n$ . **B.** Simplified molecular picture of the first two adsorption steps, depicting film deposition starting with a positively charged substrate. **C.** Chemical structures of two typical polyelectrolytes, the sodium salt of poly(styrene sulfonate) and poly(allylamine hydrochloride).

Nevertheless, glass slide, silicon or any other macroscopic object are not suitable as platforms for the fabrication of miniaturized sensors for SERS. A suitable alternative involve the utilization of submicrometer or micromaterials as substrates (silica or latex

beads). Such composite material present long-term optical stability, and moreover exploit the main advantages of colloidal and film SERS substrates because: <sup>68</sup>

- (1) Stability issues are overcome after the deposition of the silver colloids. Such substrates provide long-term colloidal stability, allowing for extensive cleaning if necessary.
- (2) The particles deposited on the substrate's surface are in close contact with one another while in suspension, thus generating stable hot spots that yield high SERS intensities
- (3) Permits the storage of the material for extended time with no negative impact on the colloidal stability and optical properties.

#### 1.4. SERS sensing

SERS as a powerful molecular spectroscopic technique with the capability of ultradetection sensing is a reliable analytical tool that is expanding its realm of applications from diagnosis and biomedical applications to environmental monitoring with potential multiplexing and real time analysis. In serious medical issues the fast and accurate detection of the pathogen is literally a matter of life and death. SERS biosensors can be applied in the detection of biological samples and diseases, including various types of cancer,<sup>69</sup> prionic diseases such as Alzheimer and Parkinson.<sup>70</sup> The potential substitution of the time consuming and more costly traditional immunological detection assays which employ antibody methods as the enzyme-linked immunosorbent assay (ELISA) by SERS immunosensors with the ability to provide information in the complex biological environments with minimum sample preparation and high spatial resolution.

Direct detection of the target analyte is the most ordinary way for the SERS detection. Upon chemisorption of the analyte to the plasmonic surface, the SERS spectrum retrieved is unique as a fingerprint for each molecule. Direct sensing is adequate for multiplex analysis which allows simultaneous measurements of various target analytes in a single cycle of the assay within the same sample where the particle itself is the sensing element. Multiplex analysis can also be applied for indirect detection, where the particles are surface functionalized with one or more ligands with the ability to react selectively at the existence of certain substances or encoded particles, that act as cellular or molecular labels.<sup>71</sup> Direct sensing provides a flexible platform and can lead to ultrasensitive detection. On the contrary, there are cases

where many molecular species co-exist as in the case of the complex nature of the biological fluids. A purification step is needed before SERS analysis otherwise the result data are almost impossible to interpret. An alternative to this problem is the direct contact between the sensing colloidal composite and the fluid of interest, followed by separation from the fluid by means of a suitable physical or chemical property, such as magnetism or simply centrifugation, and finally washing and analysis. This type of sensing is indirect because the changes induced on the structure of the antibody are due to the coupling of the antigen.

SERS spectroscopy can be applied for the detection of inorganic molecules and ions through direct and indirect means. Inorganic atomic species do not display vibrational signal, making their identification by a molecular vibrational spectroscopy like SERS, impossible. Nevertheless, it is well known that there is interaction between the noble metals and the heavier halogens (Cl, Br, and I) and chalcogens (S, Se, Te). These species are transformed into molecules, because they form surface complexes with the gold or silver and therefore can be analyzed by SERS. Their electron-rich nature and their proximity to the optical enhancer are the reasons for their SERS activity.

An indirect approach consists of the use of a molecular probe with high SERS cross-section that is directly adsorbed onto the plasmonic surface and undergoes significant changes upon interaction with the inorganic ion. This strategy is in the same directive, as it has been successfully employed in biosensors mentioned before. The first report in the literature for atomic ion detection described the use of gold nanoshells for the measurement of protons (pH value) upon ionization/deionization of the carboxylic group of 4-mercaptobenzoic acid (MBA) when exposed to solutions with different pH values. After this and due to the ever-increasing interest, a number of publications reported the use of organic ligands for the indirect SERS identification of atomic cations, such as Zn(II) with 4-(N-piperazinyl)terpyridine dithiocarbamate, Cu (II), Zn(II), Hg(II), and Pb(II) with MBA, Hg(II) and Cd(II) with trimercaptotriazine, Cu(II) with 2-mercaptobenzimidazole, or Cl<sup>-</sup> with the 2-(2-(6-methoxyquinoliniumchloride)ethoxy) ethanamine hydrochloride (amino-MQAE). The quantification capability of this method depends on the molecular probe used to interact with the ionic atom achieving detection down to the picomolar regime.<sup>72</sup>

One of the main challenges is the transition of these laboratory level sensors to effective and practical widespread tools. Advances in the field are still needed in order to overcome issues that arise when working with complex media such the real life



samples, including natural and waste waters, that require some form of sample preparation even in the case of indirect sensing.

## 1.5. Bibliography

1. G. Landsberg G. and L. Mandelstam L., "Eine Neue Erscheinung Bei Der Lichtzerstreuung in Krystallen," *Naturwissenschaften*, 1928, 16, 557.
2. Raman C. V. and Krishnan K. S., "A New Type of Secondary Radiation," *Nature*, 1928, 121, 501–502.
3. Smekal Adolf, "Zur Quantentheorie der Dispersion," *Naturwissenschaften*, 1923, 11, 873–875.
4. R. S. Krishnan and R. K. Shankar, "Raman Effect: History of the Discovery," *Journal of Raman Spectroscopy*, 1981, 10, 1–8.
5. McCreery Richard L., "Raman Spectroscopy for Chemical Analysis"
6. Le Ru, E. & Etchegoin, P. In *Principles of Surface-Enhanced Raman Spectroscopy and Related Plasmonic Effects*, Elsevier, 2009.
7. Nie Shuming and Emory Steven R., "Probing Single Molecules and Single Nanoparticles by Surface-Enhanced Raman Scattering", *Science*, 1997, 275, 1102–1106.
8. Kneipp Katrin, Wang Yang, Kneipp Harald, Perelman Lev T., Itzkan Irving, Dasari Ramachandra R., and Feld Michael S., "Single Molecule Detection Using Surface-Enhanced Raman Scattering (SERS)," *Physical Review Letters*, 1997, 78, 1667–1670.
9. Kim W., Safonov V. P., Shalaev V. M., and Armstrong R. L., "Fractals in Microcavities: Giant Coupled, Multiplicative Enhancement of Optical Responses," *Physical Review Letters*, 1999, 82, 4811–4814.
10. Fleischmann M., Hendra P.J., and McQuillan A.J., "Raman Spectra of Pyridine Adsorbed at a Silver Electrode," *Chemical Physics Letters*, 1974, 26, 163–166.
11. McQuillan James A., "The Discovery of Surface-enhanced Raman Scattering," *Notes and Records of the Royal Society*, 2009, 63, 105–109.
12. Jeanmaire David L. and Van Duyne Richard P., "Surface Raman Spectroelectrochemistry: Part I. Heterocyclic, Aromatic, and Aliphatic Amines Adsorbed on the Anodized Silver Electrode," *Journal of Electroanalytical Chemistry and Interfacial Electrochemistry*, 1977, 84, 1–20.

13. Albrecht M. Grant and Creighton J. Alan, "Anomalously Intense Raman Spectra of Pyridine at a Silver Electrode," *Journal of the American Chemical Society*, 1977, 99, 5215–5217.
14. Campion Alan and Kambhampati Patanjali, "Surface-enhanced Raman Scattering," *Chemical Society Reviews*, 1998, 27, 241–250.
15. Schatz George C., Young Matthew A., and Duyne Richard P., "Electromagnetic Mechanism of SERS," in *Surface-Enhanced Raman Scattering*, ed. Kneipp Katrin, Moskovits Martin, and Kneipp Harald, *Topics in Applied Physics*, 2006, 103, 19–45.
16. Gersten Joel and Nitzan Abraham, "Electromagnetic Theory of Enhanced Raman Scattering by Molecules Adsorbed on Rough Surfaces," *The Journal of Chemical Physics*, 1980, 73, 3023–3037.
17. Moskovits M., "Enhanced Raman Scattering by Molecules Adsorbed on Electrodes--a Theoretical Model," *Solid State Communications*, 1979, 32, 59–62.
18. Schatz George C., "Theoretical Studies of Surface Enhanced Raman Scattering," *Accounts of Chemical Research*, 1984, 17, 370–376.
19. Cline M. P., Barber P. W., and Chang R. K., "Surface-enhanced Electric Intensities on Transition- and Noble-metal Spheroids," *Journal of the Optical Society of America B*, 1986, 3, 15–21.
20. Wokaun A., "Surface Enhancement of Optical Fields," *Molecular Physics*, 1985, 56, 1–33.
21. Meier M., Wokaun A., and Liao P. F., "Enhanced Fields on Rough Surfaces: Dipolar Interactions Among Particles of Sizes Exceeding the Rayleigh Limit," *Journal of the Optical Society of America B*, 1986, 2, 931–949.
22. Mayer Kathryn M. and Hafner Jason H., "Localized Surface Plasmon Resonance Sensors," *Chemical Reviews*, 2011, 111, 3828–3857.
23. Ko Hyunhyub, Singamaneni Srikanth, and Tsukruk Vladimir V., "Nanostructured Surfaces and Assemblies as SERS Media," *Small* 4, 2008, 10, 1576–1599.
24. Otto A., and Mrozek I., and Grabhorn H., and Akemann W., "Surface-enhanced Raman Scattering," *Journal of Physics: Condensed Matter*, 1992, 4, 1143.
25. Campion Alan, and Kambhampati Patanjali, "Surface-enhanced Raman Scattering," *Chemical Society Reviews*, 1998, 27, 241–250.

26. Haynes Christy L., McFarland Adam D., and Van Duyne Richard P., "Surface-Enhanced Raman Spectroscopy," *Analytical Chemistry*, 2005, 77, 338 A–346 A.
27. Natan Michael J., "Concluding Remarks Surface Enhanced Raman Scattering," *Faraday Discussions*, 2006, 132, 321–328.
28. Moskovits M., "Surface Selection Rules," *The Journal of Chemical Physics*, 1982, 77, 4408–4416.
29. Le Ru E. C., Meyer M., Blackie E., Etchegoin P. G., "Advanced Aspects of Electromagnetic SERS Enhancement Factors at a Hot Spot", *Journal of Raman Spectroscopy*, 2008, 39, 1127–1134.
30. Le Ru E. C., Grand J., Félidj N., Aubard J., Lévi G., Hohenau A., Krenn J. R., Blackie E., Etchegoin P. G., "Experimental Verification of the SERS Electromagnetic Model Beyond the  $|E|^4$  Approximation: Polarization Effects," *The Journal of Physical Chemistry C*, 2008, 112, 8117–8121.
31. Barnes William L., Dereux Alain, and Ebbesen Thomas W., "Surface Plasmon Subwavelength Optics," *Nature*, 2003, 424, 824–830.
32. Alvarez-Puebla Ramón, Liz-Marzán Luis M., and García de Abajo F. Javier, "Light Concentration at the Nanometer Scale," *The Journal of Physical Chemistry Letters*, 2010, 1, 2428–2434.
33. Alvarez-Puebla Ramón A. and Luis M. Liz-Marzán, "SERS-Based Diagnosis and Biodetection", *Small*, 2010, 6, 604–610.
34. Markel V. A., Shalaev V. M., Zhang, P., Huynh W., Tay L., Haslett T. L., Moskovits M., "Near-field Optical Spectroscopy of Individual Surface-plasmon Modes in Colloid Clusters," *Physical Review B*, 1999, 59, 10903–10909.
35. Kim Won-Tae, Safonov Vladimir P., Shalaev Vladimir M., and Armstrong Robert L., "Fractals in Microcavities: Giant Coupled, Multiplicative Enhancement of Optical Responses", *Physical review Letters*, 1999, 82, 4811-4814.
36. Grésillon S., Aigouy L., Boccara A. C., and Rivoal J. C., "Experimental Observation of Localized Optical Excitations in Random Metal-Dielectric Films", *Physical Review Letters*, 1999, 82, 4520–4523.
37. Lee Seung Joon, Morrill Andrew R., and Moskovits Martin, "Hot Spots in Silver Nanowire Bundles for Surface-Enhanced Raman Spectroscopy," *Journal of the American Chemical Society*, 2006, 128, 2200–2201.

38. Otto Andreas, "What Is Observed in Single Molecule SERS, and Why?", *Journal of Raman Spectroscopy*, 2002, 33, 593–598.
39. Le Ru E. C., Meyer M., Blackie E., Etchegoin P. G., "Advanced Aspects of Electromagnetic SERS Enhancement Factors at a Hot Spot", *Journal of Raman spectroscopy*, 2008, 39, 1127-134.
40. Sharma Bhavya, Frontiera Renee R., Henry Anne-Isabelle, Ringe Emilie, Van Duyne Richard P., "SERS: Materials, Applications, and the Future," *Materials Today*, 2012, 15, 16–25.
41. Lin Xu-Feng, Ren Bin, and Tian Zhong-Qun, "Electrochemical and Surface-Enhanced Raman Spectroscopic Studies on the Adsorption and Electrooxidation of C1 Molecules on a Roughened Rh Electrode," *The Journal of Physical Chemistry B*, 2003, 108, 981–986.
42. Zheng Jian-Zhou, Ren Bin, Wu De-Yin, Tian Zhong-Qun, "Thiourea Adsorption on a Pt Surface as Detected by Electrochemical Methods and Surface-enhanced Raman Spectroscopy," *Journal of Electroanalytical Chemistry*, 2005, 574, 285–289.
43. Ren Bin, Lin Xu-Feng, Yang Zhi-Lin, Liu Guo-Kun, Aroca Ricardo F., Mao Bing-Wei, Tian Zhong-Qun, "Surface-Enhanced Raman Scattering in the Ultraviolet Spectral Region: UV-SERS on Rhodium and Ruthenium Electrodes," *Journal of the American Chemical Society*, 2003, 125, 9598–9599.
44. Muniz-Miranda Maurizio, "Surface Enhanced Raman Scattering of 4,4'-Bipyridine Adsorbed on Smooth Copper, Silver and Aluminium Surfaces Activated by Deposited Silver Particles," *Journal of Raman Spectroscopy*, 1996, 27, 435–437.
45. Xu Weigao, Xi Ling, Xiao Jiaqi, Dresselhaus Mildred S., Kong Jing, Xu Hongxing, Liu Zhongfan, and Zhang Jin, "Surface Enhanced Raman Spectroscopy on a Flat Graphene Surface," *Proceedings of the National Academy of Sciences*, 2012, 109, 9281–9286.
46. Xu Weigao, Mao Nannan, and Zhang Jin, "Graphene: A Platform for Surface-Enhanced Raman Spectroscopy", *Small*, 2013, 9, 1206–1224.
47. Musumeci Anthony, Gosztola David, Schiller Tara, Dimitrijevic Nada M., Mujica Vladimiro, Martin Darren, Rajh Tijana, "SERS of Semiconducting Nanoparticles (TiO<sub>2</sub> Hybrid Composites)", *Journal of the American Chemical Society*, 2009, 131, 6040–6041.
48. Wang Yanfei, Zhang Junhu, Jia Huiying, Li Minjie, Zeng Jianbo, Yang Bai, Zhao Bing, Xu Weiqing, Lombardi John R., "Mercaptopyrindine Surface-Functionalized CdTe

Quantum Dots with Enhanced Raman Scattering Properties”, *The Journal of Physical Chemistry C*, 2008, 112, 996–1000.

49. Livingstone Richard, Zhou Xuecong, Tamargo Maria C., Lombardi John R., Quagliano Lucia G., Jean-Mary Fleumingue, “Surface Enhanced Raman Spectroscopy of Pyridine on CdSe/ZnBeSe Quantum Dots Grown by Molecular Beam Epitaxy” *The Journal of Physical Chemistry C*, 2010, 114, 17460–17464.

50. Faraday Michael, “The Bakerian Lecture: Experimental Relations of Gold (and Other Metals) to Light,” *Philosophical Transactions of the Royal Society of London*, 1857, 147, 145–181.

51. Biswas Abhijit, Bayer Ilker S., Biris Alexandru S., Wang Tao, Dervishic Enkeleda, Faupeld Franz, “Advances in Top–down and Bottom–up Surface Nanofabrication: Techniques, Applications & Future Prospects”, *Advances in Colloid and Interface Science*, 2012, 170, 2–27.

52. Gaffet E., Tachikart M., El Kedim O., Rahouadj R., “Nanostructural Materials Formation by Mechanical Alloying: Morphologic Analysis Based on Transmission and Scanning Electron Microscopic Observations”, *International Metallography Conference Materials Characterization*, 1996, 36, 185–190.

53. Aroca R.F., Alvarez-Puebla R.A., Pieczonka N., Sanchez-Cortez S., Garcia-Ramos J.V., “Surface-enhanced Raman Scattering on Colloidal Nanostructures”, *Advances in Colloid and Interface Science*, 2005, 116, 45–61.

54. Creighton J. Alan, Blatchford Christopher G., and Albrecht M. Grant, “Plasma Resonance Enhancement of Raman Scattering by Pyridine Adsorbed on Silver or Gold Sol Particles of Size Comparable to the Excitation Wavelength,” *Journal of the Chemical Society, Faraday Transactions 2: Molecular and Chemical Physics*, 1979, 75, 790–798.

55. Kerker M., Siiman O., Bumm L. A., and Wang D.-S., “Surface Enhanced Raman Scattering (SERS) of Citrate Ion Adsorbed on Colloidal Silver,” *Applied Optics*, 1980, 19, 3253–3255.

56. Rycenga Matthew, Cobley Claire M., Zeng Jie, Li Weiyang, Moran Christine H., Zhang Qiang, Qin Dong, Xia Younan., “Controlling the Synthesis and Assembly of Silver Nanostructures for Plasmonic Applications”, *Chemical Reviews*, 2011, 111, 3669–3712.

57. Sun Yugang and Xia Younan, “Shape-Controlled Synthesis of Gold and Silver Nanoparticles”, *Science*, 2002, 298, 2176–2179.

58. Tao Andrea, Sinsermsuksakul Prasert, and Yang Peidong, "Polyhedral Silver Nanocrystals with Distinct Scattering Signatures" *Angewandte Chemie International Edition*, 2006, 45, 4597–4601.
59. Korte Kylee E., Skrabalak Sara E., and Xia Younan, "Rapid Synthesis of Silver Nanowires through a CuCl- or CuCl<sub>2</sub>- mediated Polyol Process", *Journal of Materials Chemistry*, 2008, 18, 437–441.
60. Yee Chanel, Scotti Michael, Ulman Abraham, White Henry, Rafailovich Miriam, Sokolov Jonathan, "One-Phase Synthesis of Thiol-Functionalized Platinum Nanoparticles", *Langmuir*, 1999, 15, 4314–4316.
61. Teranishi T., Hosoe M., Tanaka T., Miyake M., "Size Control of Monodispersed Pt Nanoparticles and Their 2D Organization by Electrophoretic Deposition", *The Journal of Physical Chemistry B*, 1999, 103, 3818–3827.
62. Wu Xiaomu, Redmond Peter L., Liu Haitao, Chen Yihui, Steigerwald Michael, Brus Louis, "Photovoltage Mechanism for Room Light Conversion of Citrate Stabilized Silver Nanocrystal Seeds to Large Nanoprisms", *Journal of the American Chemical Society*, 2008, 130, 9500–9506.
63. Lee P. C. and Meisel D., "Adsorption and Surface-enhanced Raman of Dyes on Silver and Gold Sols," *The Journal of Physical Chemistry*, 1982, 86, 3391–3395.
64. Whitesides George M. and Grzybowski Bartosz, "Self-Assembly at All Scales," *Science*, 2002, 295, 2418–2421.
65. Kotov Nicholas A., Dekany Imre, and Fendler Janos H., "Layer-by-Layer Self-Assembly of Polyelectrolyte-Semiconductor Nanoparticle Composite Films," *The Journal of Physical Chemistry*, 1995, 99, 13065–13069.
66. Decher Gero, "Fuzzy Nanoassemblies: Toward Layered Polymeric Multicomposites," *Science*, 1997, 277, 1232–1237.
67. Schmitt Johannes, Decher Gero, Dressick Walter J., Brandow Susan L., Geer Robert E., Shashidhar R., Calvert Jeffrey M., "Metal Nanoparticle/polymer Superlattice Films: Fabrication and Control of Layer Structure," *Advanced Materials*, 1997, 9, 61–65.
68. Spuch-Calvar Miguel, Rodríguez-Lorenzo Laura, Puerto Morales M., Álvarez-Puebla Ramón A., Liz-Marzán Luis M., "Bifunctional Nanocomposites with Long-Term Stability as SERS Optical Accumulators for Ultrasensitive Analysis", *The Journal of Physical Chemistry C*, 2008, 113, 3373–3377.

69. Grubisha DS, Lipert RJ, Park HY, Driskell J, Porter MD., "Femtomolar Detection of Prostate-Specific Antigen: An Immunoassay Based on Surface-Enhanced Raman Scattering and Immunogold Labels", *Analytical Chemistry*, 2003, 75, 5936–5943.
70. Alvarez-Puebla Ramón A., Agarwal Ashish, Manna Primit, Khanal Bishnu P., Aldeanueva-Potel Paula, Carbó-Argibay Enrique, Pazos-Pérez Nicolas, Vigderman Leonid, Zubarev Eugene R., Kotova Nicholas A., and Liz-Marzán Luis M., "Gold Nanorods 3D-supercrystals as Surface Enhanced Raman Scattering Spectroscopy Substrates for the Rapid Detection of Scrambled Prions", *Proceedings of the National Academy of Sciences*, 2011, 108, 8157-8161.
71. Rodriguez-Lorenzo Laura, Fabris Laura, and Alvarez-Puebla Ramon A., "Multiplex Optical Sensing with Surface-enhanced Raman Scattering: A Critical Review," *Analytica Chimica Acta*, 2012, 745, 10–23.
72. Alvarez-Puebla Ramón A. and Liz-Marzán Luis M., "SERS Detection of Small Inorganic Molecules and Ions", *Angewandte Chemie International Edition*, 2012, 51, 11214–11223.



## ***Chapter 2: SERS recognition of chloride (Cl<sup>-</sup>)***

---

### **Abstract**

In this chapter, we report a SERS-based ultradetection and quantification method of inorganic atomic ions some of which, the halogens, are of environmental and biological importance. Chloride sensing is demonstrated by monitoring the vibrational changes introduced upon interaction with a Cl<sup>-</sup>-sensitive probe supported onto a nanostructured silver-coated silica microbead. The engineered particles play an important role in the detection, as they primarily constitute a highly plasmonic platform because they hold a dense collection of SERS hot spots as well as a colloidal stable substrate to support the high SERS cross-section Cl<sup>-</sup>-sensitive capping agent. Our results contribute toward the fabrication of microsensors for fast ultradetection and quantification of representative atomic ions of biological importance. Additionally, limiting the dimensions of the transduction element to that of the discrete microparticles rather than other conventional SERS substrates, allows the study inside the living organisms.

## 2.1 Introduction

Nowadays, SERS spectroscopy has proven to be an ultrasensitive, ultra-fast and universal analytical tool, which can provide fingerprint-like information of the molecule under examination. The enhancement of the Raman signal in SERS leads to very sensitive probing of chemical structure and composition, and the nanometer-scale spatial confinement of the effect enables highly localized measurements. Until recently this sensitive type of vibronic spectroscopy was restricted to molecular analytes with high affinity towards the conventional plasmonic substrates under certain experimental conditions.<sup>1</sup> Consequently, the detection of atomic species by SERS has been very limited partly, due to their very small Raman scattering cross-section and the absence of vibrational modes in such systems. Another factor is that this field is already dominated by well established analytical methods that are commonly used for this type of task. For instance, detection and quantification of metal cations is conducted by atomic absorption or emission spectroscopy,<sup>2</sup> anions are detected by ion exclusion chromatography,<sup>3</sup> electrochemical methods,<sup>4</sup> electronic absorption or emission (colorimetry),<sup>5</sup> and resonance Raman scattering.<sup>6</sup> Notwithstanding these techniques usually provide ultradetection, yet, most of them are destructive, require a substantial amount of sample as well as direct interactions between the sample and the sensor.<sup>7</sup>

Inorganic halide species continue to be the subject of numerous studies and new analytical methods are still challenging, due to their abundance in nature and the key role that possess in living organisms. As far as the five halogens are concerned, only four of them, fluorine (F), chlorine (Cl), bromine (Br) and iodine (I) are of practical importance. Hence, the determination of the halide levels in nature, has always attracted attention, for environmental monitoring purposes such as pollution in air and waters, as well as monitoring halide deficiencies in natural resources, such as in soils and drinking water. For example, chloride in the form of salt water is a major contaminant of ground water. Therefore, its identification and quantification are important, so, monitoring chloride levels in drinking water for instance, is concerned. Monitoring of chloride diffusion into steel (can cause corrosion of steel at concentrations as low as 600–900  $\mu\text{g ml}^{-1}$  and potentially structural failure), reinforced concrete structures, from ground water, is also of great importance. Inorganic electrolytes such as halide ions are also present in human physiology and are necessary for vital cellular activity. Cystic fibrosis is a good example of illness associated with chloride abnormalities. In particular, the illness is characterized by a high chloride concentration in a patient's sweat and saliva as compared to non-cystic

fibrosis patients.<sup>8</sup> There is also a vast interest in determining the halide levels ranging from everyday products (toothpastes, vegetables, milk, pharmaceutical products) to industrial processes (pollutant in industrial wastes and waste waters). Therefore halide sensing concentrates a lot of interest on the fields of human biology, everyday consuming products and for environmental monitoring.

Since nanoengineering brings a vast impact on fields such as sensing and biomedicine, the design of novel sensing systems which are more effective, less time consuming, without the need of pretreatment, allowing identification in complex media, is more than promising.<sup>9,10</sup> As already mentioned above, SERS spectroscopy is an ultrasensitive analytical tool in which the Raman signal of the molecular probe is dramatically enhanced when in close proximity in a noble metal nanostructure.<sup>11</sup> Even though SERS is a molecular technique, yet, there are several published works that exploit SERS spectroscopy for the detection of atomic species utilizing different approaches. Such is the case of the SERS Hg<sup>II</sup> detection utilizing the high affinity between the mercury and the gold.<sup>12</sup> Another method of ionic atoms detection strategy lies in the aggregation of particles, which were primarily functionalized with a specific ion receptor and a high cross-section Raman reporter. The induced aggregation as a result of the ion concentration, is registering increased SERS signal of the Raman reporter due to the formation of hot-spots. Detection of Cd<sup>II</sup> with a Cd<sup>II</sup> chelating polymer, As<sup>III</sup> with glutathione, Hg<sup>II</sup> with a DNA aptamer, or Hg<sup>II</sup> with Bismuthiol II are typical examples.<sup>7,13,14,15</sup> Indirect SERS methods utilizing a molecular probe that undergoes significant geometrical or electronic changes upon interaction with the desired analyte, have also been reported. Especially those regarding biosensors using antibodies or nucleic acid aptamers as the active interlayer for the indirect detection of proteins and other analytes.<sup>16,17,18</sup> The first published work in literature regarding indirect SERS detection of atomic ions, described the use of optimized SERS nanoprobe as the gold nanoshells for the measurement of protons (pH) upon ionization/deionization of the carboxylic group of 4-mercaptobenzoic acid (MBA), when exposed to solutions with different pH.<sup>19</sup> The use of MBA as a pH-sensitive probe had been widely used for internal pH monitoring in living cells.<sup>20,21</sup> Examples of other indirect SERS determination of atomic cations are Zn<sup>II</sup> with 4-(N-piperazinyl)terpyridine dithiocarbamate, Cu<sup>II</sup>, Zn<sup>II</sup>, Hg<sup>II</sup>, and Pb<sup>II</sup> with MBA, Hg<sup>II</sup> and Cd<sup>II</sup> with trimercaptotriazine, Cu<sup>II</sup> with 2-mercaptobenzimidazole.<sup>7,22,23,24,25</sup>

Nevertheless, a major drawback in such kind of indirect SERS strategies may be the lack of colloidal stability upon organic ligand surface modification of the nanoparticles, which are very sensitive to any change in their environment and as a result, aggregation may occur. To overcome this, an alternative approximation in the fabrication of the sensor is suggested exploiting the use of nanostructured thin films yet in a miniaturized level. In order to achieve this, a highly plasmonic surface is generated over the surface of submicrometer tailored materials used as a stable platform containing a dense collection of hot spots.<sup>26,27</sup>

In the context of this chapter, we demonstrate the use of surface-enhanced Raman scattering spectroscopy for the indirect, quantitative detection of atomic anions. We developed a sensor based on the vibrational changes induced by the interaction of chloride with a Cl-sensitive molecular probe that has a high SERS cross-section. A plasmonic platform consisting of silver-coated, micrometer-sized silica beads was developed, that can overcome undesired effects such as, colloidal aggregation upon self-assembly of the Cl-sensitive probe, while providing a dense collection of hot spots. Minute amounts of chloride down to the pM regime were quantitatively detected through the direct comparison of the SERS spectra of the ligand before and after interaction with chloride in aqueous solution.<sup>27</sup>

## 2.2 Experimental details

### 2.2.1 Chemicals

Silica microparticles, with 1.16  $\mu\text{m}$  diameter, were purchased from microParticles GmbH. All other chemicals were purchased from Aldrich and used without further purification. Water was purified using a Milli-Q system (Millipore).

### 2.2.2 Silica Bead Functionalization and Synthesis and Adsorption of Gold Seeds ( $\text{SiO}_2@Au$ )

Gold sols were prepared according to the standard sodium citrate reduction method, by adding 2 mL of 1 wt % sodium citrate solution to a 100 mL boiling solution of  $\text{HAuCl}_4$  ( $5 \times 10^{-4}$  M) under stirring and additional boiling for 15 min.<sup>28</sup> This method produces a deep-red dispersion of gold nanoparticles (AuNPs) with an average diameter of around 15 nm. Polyelectrolyte-coated  $\text{SiO}_2$  particles were prepared by

adding 1 mL of polyethyleneimine (PEI) ( $M_w = 25000$ ,  $1 \text{ mg mL}^{-1}$  in  $\text{NaNO}_3$  0.5 M) under weak sonication to 1 mL of the silica particles in water ( $1.6 \text{ g L}^{-1}$ ). PEI adsorption was allowed for 1 h and then excess PEI was removed by three repeated centrifugation cycles (10 min, 3500 rpm). Polystyrene sulfonate (PSS) ( $MW = 1000000$ ,  $1 \text{ mg mL}^{-1}$  in  $\text{NaNO}_3$  0.5 M) was then deposited onto the PEI-coated silica particles under the same conditions, followed by deposition of an additional layer of PEI which forms the outermost layer. Adsorption of the gold seeds was carried out by adding 5 mL of AuNPs colloid solution ( $5 \times 10^{-4} \text{ M}$ ) to 5 mL of functionalized  $\text{SiO}_2$  particles ( $1.16 \mu\text{m}$ ,  $1.6 \text{ g L}^{-1}$ ). The mixture was sonicated for 15 min. After 1 h the sample was washed by centrifugation ( $4 \times 3500 \text{ rpm}$ , 30 min) to remove gold nanoparticles that did not adsorb on the silica surface and redispersed in 5 mL of water to obtain a final  $\text{SiO}_2@Au$  concentration of  $1.6 \text{ g L}^{-1}$ .

### 2.2.3 Silver Growth on the Gold Seeds ( $\text{SiO}_2@Au@Ag$ )

Epitaxial growth of silver on the preformed gold seeds was carried out as follows:  $\text{SiO}_2@Au$  ( $1 \text{ mL}$ ,  $1.6 \text{ g L}^{-1}$ ) was added to  $2.75 \text{ mL}$  of glycine ( $0.4 \text{ M}$ ) buffer solution at pH 9.5. Then,  $281.3 \mu\text{L}$  of ascorbic acid  $0.1 \text{ M}$  and a variable concentration of  $\text{Ag}_2\text{SO}_4$  ( $15.2 \text{ mM}$ ) was added under weak sonication to reach final silver concentrations ranging from  $9.3 \times 10^{-4}$  to  $3.7 \times 10^{-3} \text{ M}$ . After 30 min the reduction was finished and the sample was washed by centrifugation ( $4 \times 3500 \text{ rpm}$ , 30 min) and redispersed in  $1 \text{ mL}$  of water to obtain a final concentration in particles of  $1.6 \text{ g L}^{-1}$ .

### 2.2.4 Synthesis of 2-(2-(6-Methoxyquinoliniumchloride)ethoxy)- thanaminehydrochloride (Amino-MQAE)

2-Aminoethoxyethanol was protected at the amino function by reaction with phthalic anhydride in toluene under reflux overnight to yield the corresponding phthalimide. Subsequently, the alcohol group was brominated in a one-pot reaction by adding phosphorus tribromide under cooling at  $0 \text{ }^\circ\text{C}$ . After being stirred at room temperature (RT), the mixture was poured into water, extracted with toluene, and recrystallized to yield 2-[2-(20-bromoethoxy)ethyl]isoindoline-1,3-dione. The phthalimide-protected amino-MQAE was synthesized by heating 6-methoxyquinoline with 2-[2-(20-bromoethoxy)ethyl] isoindoline-1,3-dione at  $110 \text{ }^\circ\text{C}$  for 3 h. The alkylation product was recrystallized from acetone. Deprotection of the phthalimide was achieved by heating in hydrochloric acid overnight; the formed phthalic acid was separated by

filtration. After recrystallization from methanol/acetone, the amino-MQAE was obtained as light yellow crystals.

### 2.2.5 Material Characterization

UV-vis-NIR spectra were recorded using an Agilent 8453 diode array spectrophotometer. XPS analysis of the samples was performed using a VG Escalab 250 iXL ESCA instrument (VG Scientific), equipped with aluminum KR 1.2 monochromatic radiation at 1486.92 eV X-ray source. Binding energies (BEs) were referenced to the C1s on unspattered surfaces. The atomic concentrations were determined from the XPS peak areas using the Shirley background subtraction technique and the Scofield sensitivity factors. Transmission electron microscopy was carried out using a JEOL JEM 1010 microscope operating at an acceleration voltage of 100 kV. Scanning electron microscopy (SEM) images were obtained with a JEOL JSM 6700F field-emission microscope, using either lower secondary electron image (LEI) or secondary electron image (SEI) detectors.

### 2.2.6 Theoretical Calculations

Geometry optimizations at the DFT level were carried out with the Gaussian 09 (Revision A.02) suite of programs. Computations with the Minnesota hybrid functional M052X by Zhao and Truhlar ensure a high level of theory and an accurate estimation of the noncovalent interactions.<sup>29</sup> The basis set used was a 6-31+G\* basis set. Geometrical convergence was obtained with at least a tight criterion. The terminal amino group of the amino-MQAE was fixed to represent the bond between the nitrogen atom and the metallic surface.<sup>27</sup>

### 2.2.7 Fluorescence and Surface-Enhanced Raman Scattering Spectroscopy

Raman and SERS experiments were conducted in a micro- Renishaw InVia Reflex system. The spectrograph uses high resolution gratings (1800 or 1200 grooves  $\text{cm}^{-1}$  for the visible or NIR, respectively) with additional band-pass filter optics, a confocal microscope and a 2D-CCD camera. Excitation was carried out at different energies, using a laser line at 532 nm. Measurements were made using a macrosampler accessory. The  $\text{SiO}_2@Au@Ag$ -amino-MQAE was desalted prior to fluorescence or SERS spectroscopy with a PD10 desalting column (Sigma, no. 54805) to remove eventual chloride contaminants. For the SERS characterization of the material, 10  $\mu\text{L}$  of benzenethiol ( $10^{-4}$  M) were added to 1 mL aliquots ( $0.16 \text{ mg mL}^{-1}$ ) of

the SiO<sub>2</sub>@Au@Ag suspension with different silver content to reach a final analyte concentration of 10<sup>-6</sup> M. Upon evaluation of the SERS intensity as a function of silver content, variable concentrations of amino-MQAE, from 10<sup>-3</sup> to 10<sup>-13</sup> M, were self-assembled onto the selected material, and its detection limits were determined by SERS. Subsequently, variable concentrations of chloride ions (from 10<sup>-10</sup> to 10<sup>-11</sup> M) were added to the SiO<sub>2</sub>@Au@Ag-amino-MQAE sensor and studied by SERS using a 532nm laser line. For quantitative analysis, bands were deconvoluted by Lorentzian shape, where the band position and the full widths at half maxima were fixed after applying a linear baseline (figure 2.8.A).<sup>30</sup> Fluorescence spectra were recorded on a Fluorolog fluorescence spectrometer (Horiba) at sodium chloride concentrations from 0 to 140 mM in 10 mM steps. The sample stock solution was mixed with sodium chloride stock solutions (1:1) in a plastic reaction vessel before filling the mixture into a quartz cuvette. The fluorophore (amino-MQAE) was excited at 350nm.

## 2.3 Results and discussion

This section deals with the fabrication of a novel SERS sensor for the identification and quantification of the chloride down to the picomolar regime. The fabrication process of the SiO<sub>2</sub>@Au@Ag is a multistep synthetic route as illustrated in figure 2.1.A. The composite colloidal particles are synthesized starting from bare silica beads which are surface modified according to the well-known LbL assembly protocol in which sequential layers of opposite charged polyelectrolytes are deposited over the surface of the negatively charged silica beads (figure 2.1.B). At the external polyelectrolyte layer follows the adsorption of citrate stabilized AuNPs (figure 2.1.C), which is a crucial step in order to achieve the epitaxial overgrowth with Ag<sup>+</sup> over the AuNPs (figure 2.1.D).<sup>31,32</sup> Tuning of the localized surface plasmon resonance (LSPR) is attained by varying the amount of the added Ag<sup>+</sup> which alters the final size distribution of the nanoparticles and consequently their interspace distances, which directly affects the interparticle plasmon coupling between neighboring particles.<sup>33</sup>

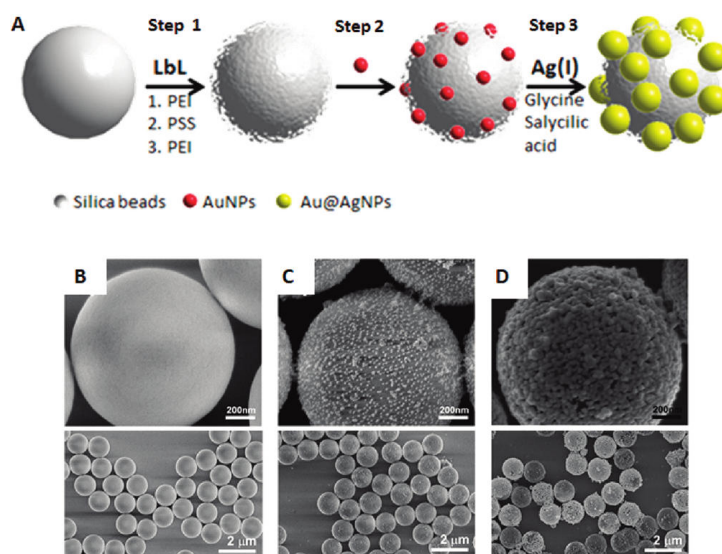


**Figure 2.1.** (A) Schematic drawing for the fabrication of micrometer-sized plasmonic hybrid materials. Scanning electron microscopy (SEM) images of the starting silica beads (B), after coating with gold nanoparticles (C), and after silver overgrowth on the gold nanoparticles (D).

From the X-ray photoelectron spectroscopy (XPS) analysis proves the bimetallic nature of the nanoparticles. After the silver growth, are only observed the characteristic 3d bands of metallic silver while the characteristic 4f bands of metallic gold are notably decreased from the previous step, suggesting the nature of the particles as segregated (core-shell) nanoalloys rather than solid solutions as can be seen in figure 2.2.

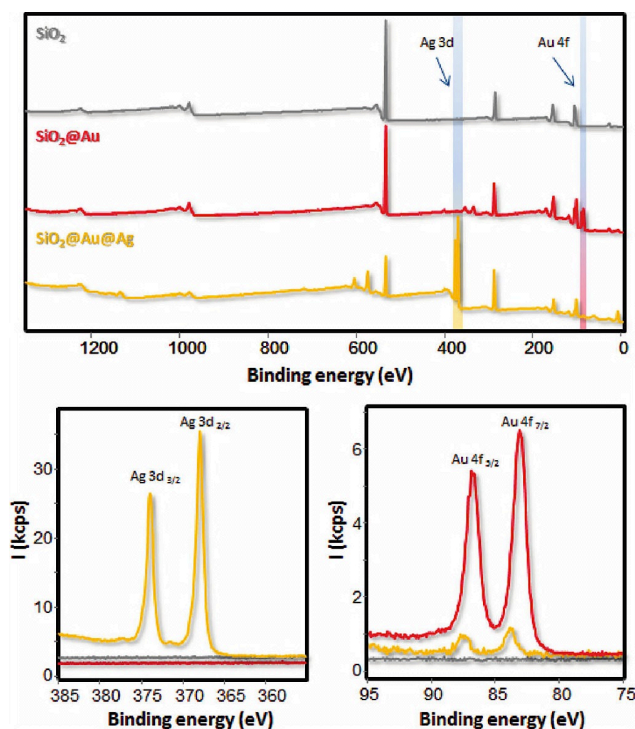


**Figure 2.2.** Survey and HR-XPS spectra of  $\text{SiO}_2$ ,  $\text{SiO}_2@Au$ , and  $\text{SiO}_2@Au@Ag$ .



The optical characterization of the samples at each stage by UV-vis spectroscopy (figure 2.3.) show no LSPR band for to the bare silica beads, upon gold coating appears a weak LSPR band centered at 535 nm and finally after the silver overgrowth this band maximum is blue-shifted and notably increases in intensity and broadens due to the interparticle plasmon coupling, which is consistent with the higher energy plasmon resonances in AgNPs.<sup>33</sup>

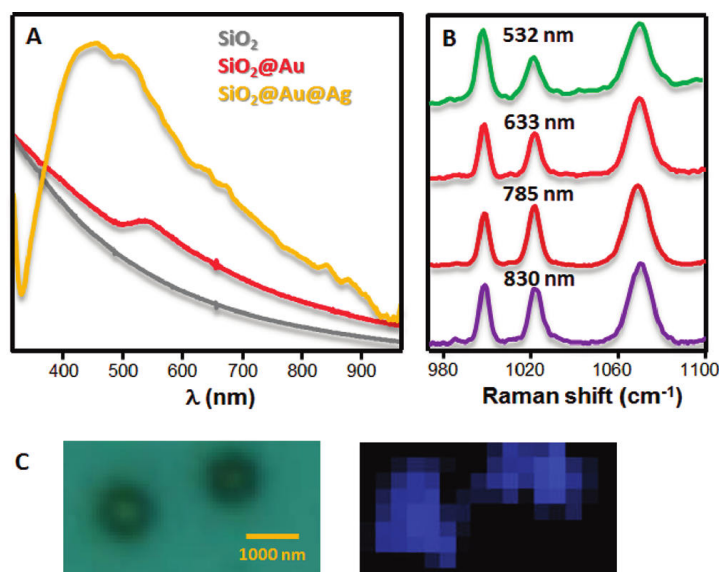


**Figure 2.3.** (A) UV-vis spectra of SiO<sub>2</sub>, SiO<sub>2</sub>@Au, and SiO<sub>2</sub>@Au@Ag beads. (B) SERS spectra of BT on SiO<sub>2</sub>@Au@Ag upon excitation with different laser lines, from the green to the NIR. (C) White light and SERS (band at 999 cm<sup>-1</sup>) images of two single SiO<sub>2</sub>@Au@Ag beads.

In order to test the optical enhancing properties of the materials we performed SERS measurements using benzenethiol (BT) as probe molecule. It is clearly shown in figure 2.3.B that the silver particles lead to strong SERS signals characteristic of BT vibrational modes corresponding to the ring breathings (999 and 1073 cm<sup>-1</sup>) and the CH in-plane bending (1023 cm<sup>-1</sup>), in a broad excitation window from the green (532 nm) to the NIR (830 nm). In figure 2.3.C is presented the SERS mapping of single beads which proves the homogeneous SERS signal over the surface of one single bead making it sufficient to obtain a high quality spectrum.

Figure 2.4.A presents the other fundamental component of the sensing device, the chloride sensitive organic probe MQAE.<sup>34</sup> This is the amino-modified version of MQAE, 2-(2-(6-methoxyquinoliniumchloride)ethoxy)-ethanamine-hydrochloride (amino-

MQAE), an organic fluorophore with a side chain containing a terminal amino group, which is necessary for the covalent bonding of the molecule to the metallic surface. Amino-MQAE is characterized by an electronic absorption band with maxima centered at 315 and 341 nm and when excited with the appropriate light (350 nm) yields a strong emission band with a maximum located at 440 nm (figure 2.4.B). Upon interaction of amino-MQAE and chloride the fluorescence gets quenched. This decrease in the emitted fluorescence intensity is correlated with the concentration of the  $\text{Cl}^-$  as shown in figure 2.4.C and can get no further than the micromolar regime (figure 2.4.D).

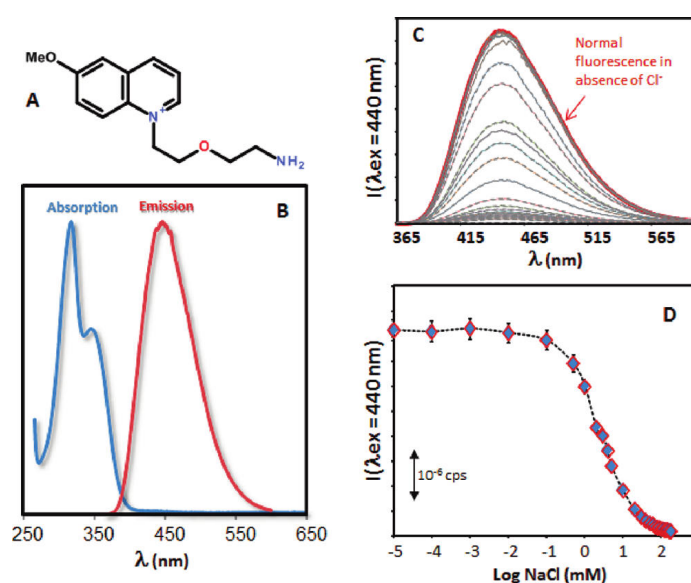


**Figure 2.4.** (A) Chemical structure of (amino-MQAE). (B) Electronic absorption and emission spectra of amino-MQAE. (C) Emission spectra of amino-MQAE as a function of chloride concentration. (D) Representative plot of the change of emission intensity versus  $\text{p}[\text{Cl}^-]$

#### Picomolar SERS ultradetection of chloride

The SERS remote detection process of the  $\text{Cl}^-$  is schematically illustrated in figure 2.5, where are also shown the Raman and SERS spectra of the amino-MQAE in the absence and in the presence of an equimolar concentration of chloride. The concept was that upon interaction of the amino-MQAE with the chloride, the induced changes will be directly reflected to the spectral pattern of the molecular probe when compared before and after interaction. The Raman signal obtained from the amino-MQAE contain mainly the in-plane vibrational modes, specifically ring stretchings

(1483, 1444, and  $1397\text{ cm}^{-1}$ ), and bendings ( $1370$  and  $1232\text{ cm}^{-1}$ ), while the out-of-plane modes carry a low vibrational Raman intensity, including CH waggings ( $830$ ,  $717\text{ cm}^{-1}$ ), ring deformations ( $578\text{ cm}^{-1}$ ), and ring waggings ( $438\text{ cm}^{-1}$ ). Notably the band at  $1086\text{ cm}^{-1}$  can be ascribed to CO stretching.

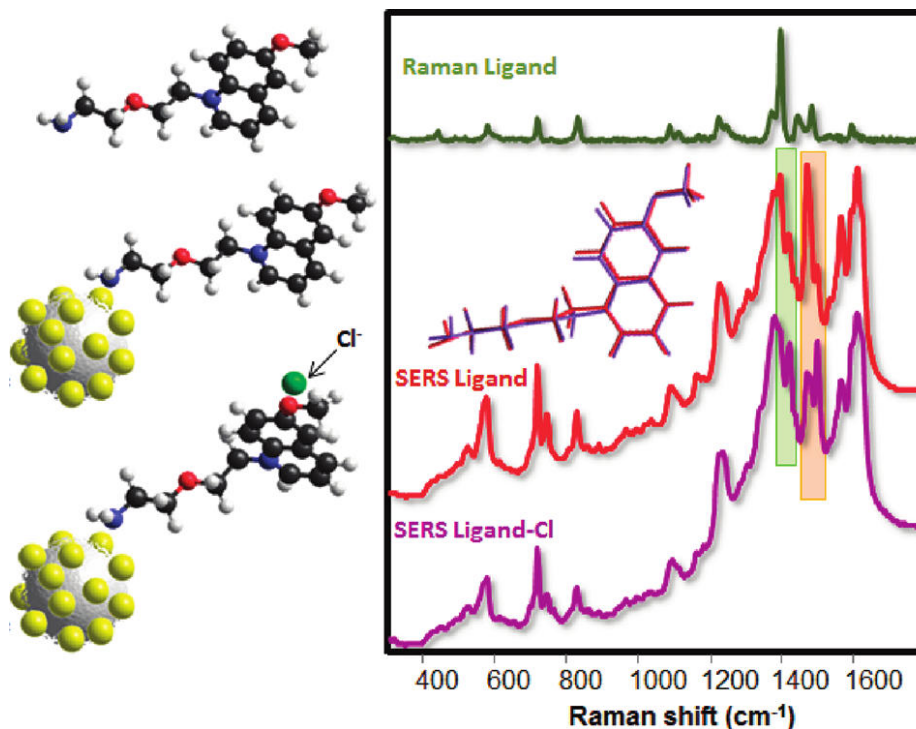
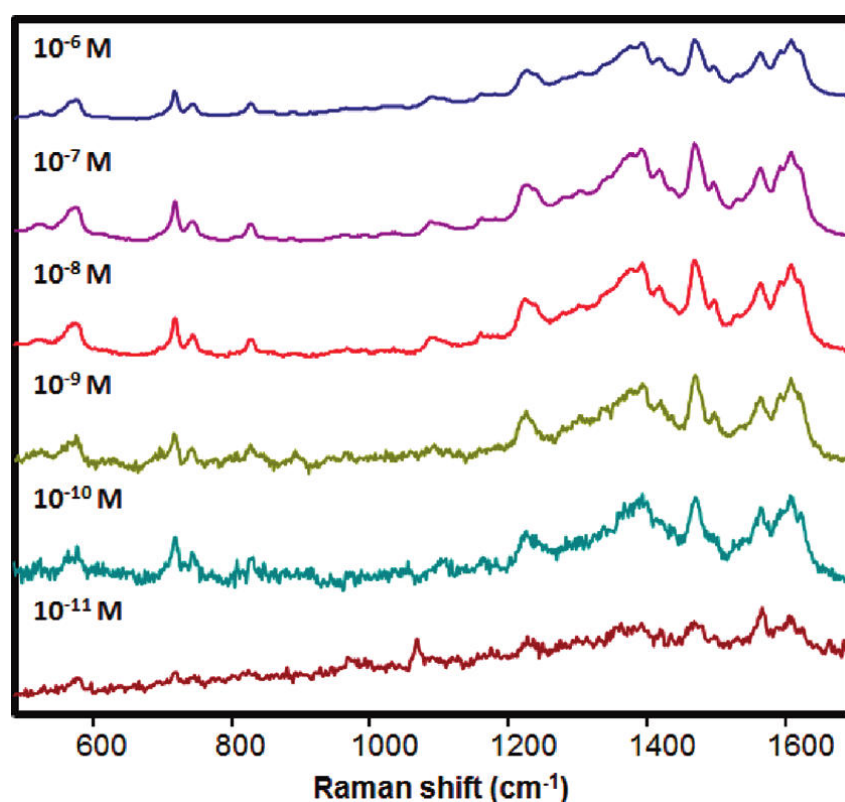


**Figure 2.5.** Left: Schematic representation of the detection process. Right: Raman and SERS spectra of amino-MQAE and SERS spectrum of amino-MQAE in the presence of an equimolar concentration of chloride ( $10^{-6}\text{ M}$ ). Optimized molecular geometry of amino-MQAE (at the M052X 6-31+G\* theory level) in the presence (blue) and absence (red) of  $\text{Cl}^-$ . Samples were excited with a 532 nm laser line.

The SERS spectrum of the amino-MQAE is dominated by the strong relative intensity of all the in-plane vibrational frequencies of the ring stretching and C-H bending in the  $1000\text{-}1650\text{ cm}^{-1}$  region, when compared to those corresponding to out-of-plane modes. These results allow the assumption that the ligand is bonded through the terminal amino group with its aromatic chromophore perpendicular to the silver surface allowing the chloride to interact with the N-heteroring promoting a series of geometrical and electronic changes in the ligand. The SERS spectrum of the amino-MQAE at the presence of the chloride concentrates the vibrational changes in the in-

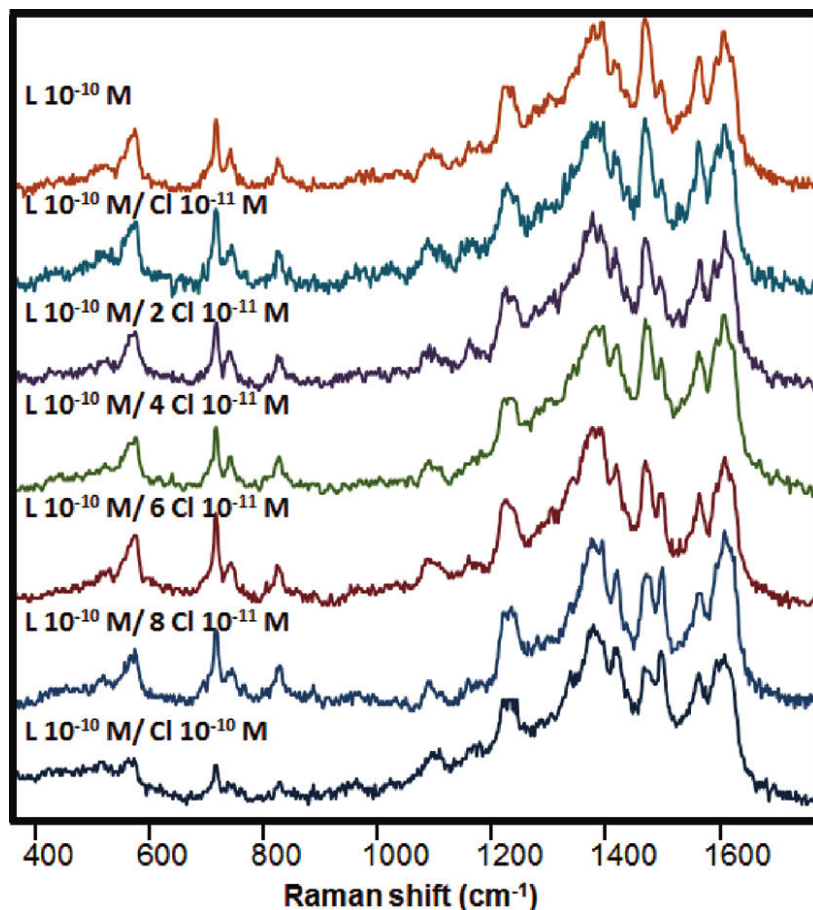
plane region of the spectra (from  $1200\text{ cm}^{-1}$  upward) and especially at those with a strong component of the C-N bond ( $1479$  and  $1497\text{ cm}^{-1}$ ).

Considering all the above information, the following stage is to study the detection limits of the amino-MQAE as shown in figure 2.6. Such a thing allow us to define the lowest concentration yet thoroughly satisfied quality spectrum to further study and quantify the ligand-Cl interaction. The amino-MQAE is detectable until concentration  $10^{-11}\text{ M}$ , however due to the low signal to noise ratio of the spectrum the concentration of  $10^{-10}\text{ M}$  was chosen to perform the quantitative identification of the Cl<sup>-</sup>.



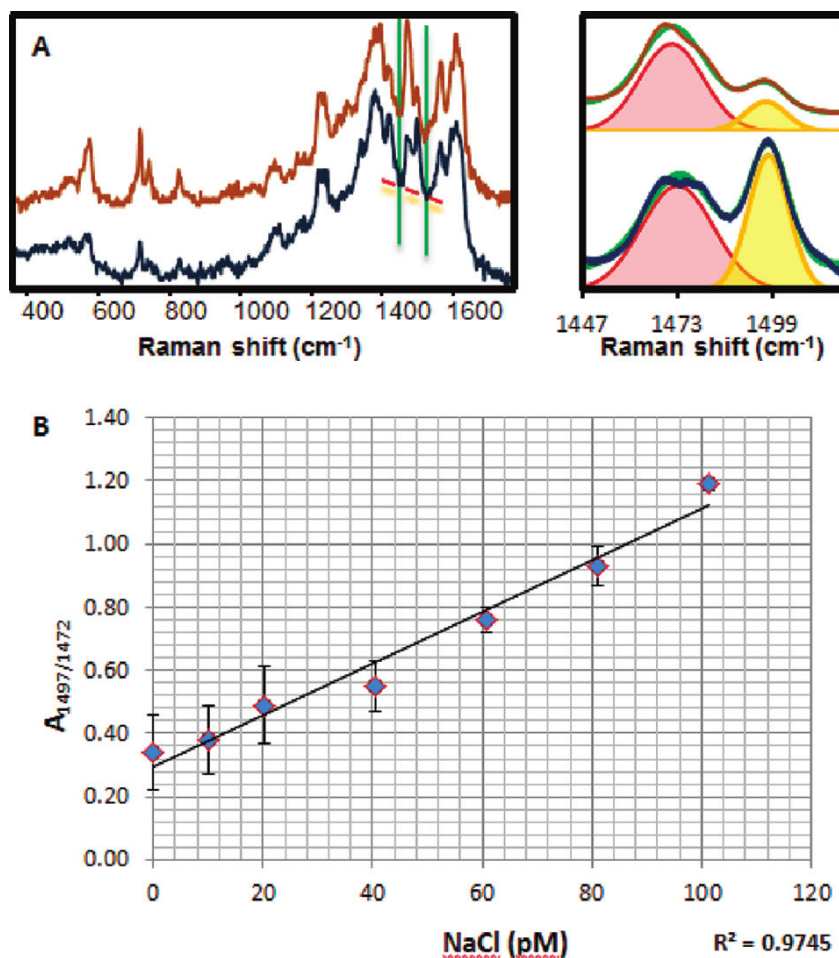
**Figure 2.6.** SERS spectra of amino-MQAE as a function of its own concentration in solution.

Figure 2.7. shows that the intensity of the vibrational modes related with the N-heteroring as the stretchings at  $1479$  and  $1497\text{ cm}^{-1}$ , decreases as the chloride concentration increases. This trend is fully recognizable at concentrations as down as  $2 \times 10^{-11}\text{ M}$ , which is equivalent to the picogram regime.



**Figure 2.7.** SERS spectra of amino-MQAE (ligand L)  $10^{-10}$  M with increasing concentrations of chloride from  $10^{-11}$  to  $10^{-10}$  M.

The concentration of chloride in the sample can be retrieved indirectly simply by comparing the ratio between the bands that hold the most distinguished changes. The bands at  $1479$  and  $1497\text{ cm}^{-1}$  were deconvoluted assuming a Lorentzian shape, where the band position and the full widths at half maxima are fixed as shown in figure 2.8.A.<sup>30</sup> Treating with the same manner all registered spectra and plotting the band area ratio between  $1479$  and  $1497$  against concentration, the result is a linear correlation, with the square of the correlation coefficient ( $r^2$ ) to reach the impressive value of  $0.9745$  which demonstrates the quantitative nature of this method of analysis (figure 2.8.B).



**Figure 2.8.** (A) SERS spectra of amino-MQAE ( $10^{-10}$  M) with and without chloride ( $10^{-10}$  M). Bands where the deconvolution was carried out are highlighted (brown and blue, experimental spectra; green, resulting spectra of coadding peak 1, red, and 2, yellow). (B) Linear plot of the 1497 and 1472  $\text{cm}^{-1}$  area ratio as a function of chloride concentration. Error bars represent the standard deviations within five replicated experiments.

## 2.4 Conclusions

In this chapter we have designed and fabricated a stable hybrid material using micrometer-sized silica platform which is uniformly coated with nanostructured silver. Such a material provides a remarkable SERS intensity as a result of the optimization of the plasmon coupling between the neighbouring silver nanoparticles, holding a dense collection of hot spots. Indirect SERS sensor with the ability of selectively recognize and quantify minute amounts of chloride, down to the picomolar regime can be attained by the vibrational response of a chloride sensitive dye.<sup>8</sup> Among the five halogens only three, chloride, bromide, and iodide, can readily be sensed by fluorescence quenching

---

methods. Among these three, only chloride is present in the cytosol of cells. Therefore, we propose this kind of sensor to be of key importance in the study of molecular and metabolic processes in living biological systems.

## 2.5 Bibliography

1. Kneipp Katrin, Moskovits Martin, and Kneipp Harald, "Surface-Enhanced Raman Scattering - Physics and Applications", Springer Berlin Heidelberg, 2006.
2. Jackson Kenneth W. and Mahmood Tariq M., "Atomic Absorption, Atomic Emission, and Flame Emission Spectrometry", *Analytical Chemistry*, 1994, 66, 252R–279R.
3. Singh Raj P., Abbas Nureddin M., and Smesko Sally A., "Suppressed Ion Chromatographic Analysis of Anions in Environmental Waters Containing High Salt Concentrations", *Journal of Chromatography A*, 1996, 733, 73–91.
4. Marco Roland, Clarke Graeme, and Pejic Bobby, "Ion-Selective Electrode Potentiometry in Environmental Analysis," *Electroanalysis*, 2007, 19, 1987–2001.
5. Lodeiro Carlos and Pina Fernando, "Luminescent and Chromogenic Molecular Probes Based on Polyamines and Related Compounds", *Coordination Chemistry Reviews*, 2009, 253, 1353–1383.
6. Fleissner Gerhard, Kozlowski Pawel M., Vargek Mária, Bryson James W., O'Halloran Thomas V., and Spiro Thomas G., "UVR Spectroscopy and Vibrational Analysis of Mercury Thiolate Compounds Resembling d10 Metal Binding Sites in Proteins" *Inorganic Chemistry*, 1999, 38, 3523–3528.
7. Alvarez-Puebla Ramón A. and Liz-Marzán Luis M., "SERS Detection of Small Inorganic Molecules and Ions", *Angewandte Chemie International Edition*, 2012, 51, 11214–11223
8. Geddes Chris D, "Optical Halide Sensing Using Fluorescence Quenching: Theory, Simulations and Applications - a Review", *Measurement Science and Technology*, 2001, 12, R53.
9. Abalde-Cela Sara, Aldeanueva-Potel Paula, Mateo-Mateo Cintia, Rodríguez-Lorenzo Laura, Alvarez-Puebla Ramón A., and Liz-Marzán Luis M., "Surface-enhanced Raman Scattering Biomedical Applications of Plasmonic Colloidal Particles", *Journal of The Royal Society Interface*, 2010.
10. Aroca R.F., Alvarez-Puebla R.A., Pieczonka N., Sanchez-Cortez S., Garcia-Ramos J.V., "Surface-enhanced Raman Scattering on Colloidal Nanostructures", *Advances in Colloid and Interface Science*, 2005, 116, 45 – 61.



11. Sperling Ralph A., Rivera Gil Pilar, Zhang Feng, Zanella Marco, and Parak Wolfgang J., "Biological Applications of Gold Nanoparticles", *Chemical Society Reviews*, 2008, 37, 1896–1908.
12. Wang Guoqing, Lim Chaesung, Chen Lingxin, Chon Hyangah, Choo Jaebum, Hong Jongin, Mello Andrew J., "Surface-enhanced Raman Scattering in Nanoliter Droplets: Towards High-sensitivity Detection of Mercury (II) Ions", *Analytical and Bioanalytical Chemistry*, 2009, 394, 1827–1832.
13. Yin Jun, Wu Tao, Song Jibin, Zhang Qian, Liu Shiyong, Xu Rong, and Duan Hongwei, "SERS-Active Nanoparticles for Sensitive and Selective Detection of Cadmium Ion (Cd<sup>2+</sup>)", *Chemistry of Materials*, 2011, 23, 4756–4764.
14. Li Jinglian, Chen Lingxin, Lou Tingting, and Wang Yunqing, "Highly Sensitive SERS Detection of As<sup>3+</sup> Ions in Aqueous Media Using Glutathione Functionalized Silver Nanoparticles", *ACS Applied Materials & Interfaces*, 2011, 3, 3936–3941.
15. Duan Junling, Yang Min, Lai Yongchao, Yuan Jingpeng, Zhan Jinhua, "A Colorimetric and Surface-enhanced Raman Scattering Dual-signal Sensor for Hg<sup>2+</sup> Based on Bismuthiol II-capped Gold Nanoparticles", *Analytica Chimica Acta*, 2012, 88–93.
16. Sanles-Sobrido Marcos, Rodríguez-Lorenzo Laura, Lorenzo-Abalde Silvia, González-Fernández África, Correa-Duarte Miguel A., Alvarez-Puebla Ramón A. and Liz-Marzán Luis M., "Label-free SERS Detection of Relevant Bioanalytes on Silver-coated Carbon Nanotubes: The Case of Cocaine", *Nanoscale*, 2009, 1, 153–158.
17. He Lili, Rodda Tom, Haynes Christy L., Deschaines Timothy, Strother Todd, Diez-Gonzalez Francisco, and Labuza Theodore P., "Detection of a Foreign Protein in Milk Using Surface-Enhanced Raman Spectroscopy Coupled with Antibody-Modified Silver Dendrites", *Analytical Chemistry*, 2011, 83, 1510–1513.
18. Kim Nam Hoon, Lee Seung Joon, and Moskovits Martin, "Aptamer-Mediated Surface-Enhanced Raman Spectroscopy Intensity Amplification", *Nano Letters*, 2010, 10, 4181–4185.
19. Bishnoi Sandra W., Rozell Christopher J., Levin Carly S., Gheith Muhammed K., Johnson Bruce R., Johnson Don H., and Halas Naomi J., "All-Optical Nanoscale pH Meter", *Nano Letters*, 2006, 6, 1687–1692.
20. Kneipp Janina, Kneipp Harald, Wittig Burghardt, and Kneipp Katrin, "One- and Two-Photon Excited Optical pH Probing for Cells Using Surface-Enhanced Raman and Hyper-Raman Nanosensors" *Nano Letters*, 2007, 7, 2819–2823.

21. Pallaoro Alessia, Braun Gary B., Reich Norbert. O., Moskovits Martin., "Mapping Local pH in Live Cells Using Encapsulated Fluorescent SERS Nanotags," *Small*, 2010, 6, 618–622.
22. Zhao Yan, Newton James N., Liu Jie, and Wei Alexander., "Dithiocarbamate-Coated SERS Substrates: Sensitivity Gain by Partial Surface Passivation", *Langmuir*, 2009, 25, 13833–13839.
23. Lee Seung Joon and Moskovits Martin, "Visualizing Chromatographic Separation of Metal Ions on a Surface-Enhanced Raman Active Medium", *Nano Letters*, 2010, 11, 145–150.
24. Zamarion Vitor M., Timm Ronaldo A., Araki Koiti, and Toma Henrique E., "Ultrasensitive SERS Nanoprobes for Hazardous Metal Ions Based on Trimercaptotriazine-Modified Gold Nanoparticles", *Inorganic Chemistry*, 2008, 47, 2934–2936.
25. Sarkar Sougata, Pradhan Mukul, Sinha Arun Kumar, Basu Mrinmoyee, Pal Tarasankar., "Selective and Sensitive Recognition of Cu<sup>2+</sup> in an Aqueous Medium: A Surface-Enhanced Raman Scattering (SERS)-Based Analysis with a Low-Cost Raman Reporter", *Chemistry – A European Journal*, 2012, 18, 6335–6342.
26. Spuch-Calvar Miguel, Rodríguez-Lorenzo Laura, Puerto Morales M., Álvarez-Puebla Ramón A., and Liz-Marzán Luis M., "Bifunctional Nanocomposites with Long-Term Stability as SERS Optical Accumulators for Ultrasensitive Analysis" *The Journal of Physical Chemistry C*, 2008, 113, 3373–3377.
27. Tsoutsis Dionysia, Montenegro Jose Maria, Dommershausen Fabian, Koert Ulrich, Liz-Marzán Luis M., Parak Wolfgang J., and Alvarez-Puebla Ramon A., "Quantitative Surface-Enhanced Raman Scattering Ultradetection of Atomic Inorganic Ions: The Case of Chloride" *ACS Nano*, 2011, 5, 7539–7546.
28. Lee P. C. and Meisel D., "Adsorption and Surface-enhanced Raman of Dyes on Silver and Gold Sols" *The Journal of Physical Chemistry*, 1982, 86, 3391–3395.
29. Zhao Yan and Truhlar Donald G., "Density Functional for Spectroscopy: No Long-Range Self-Interaction Error, Good Performance for Rydberg and Charge-Transfer States, and Better Performance on Average Than B3LYP for Ground States", *The Journal of Physical Chemistry A*, 2006, 110, 13126–13130.
30. Thomas G.J. and Agard D.A., "Quantitative Analysis of Nucleic Acids, Proteins, and Viruses by Raman Band Deconvolution", *Biophysical Journal*, 1984, 46, 763–768.

31. Decher Gero, "Fuzzy Nanoassemblies: Toward Layered Polymeric Multicomposites", *Science*, 1997, 277, 1232–1237.
32. Rodríguez-González Benito, Burrows Andrew, Watanabe Masashi, Kiely Christopher J. and Liz Marzán Luis M. "Multishell Bimetallic AuAg Nanoparticles: Synthesis, Structure and Optical Properties", *Journal of Materials Chemistry*, 2005, 15, 1755–1759.
33. Alvarez-Puebla Ramón, Liz-Marzán Luis M., and García de Abajo F. Javier, "Light Concentration at the Nanometer Scale", *The Journal of Physical Chemistry Letters*, 2010, 1, 2428–2434.
34. Engblom A.Christine and Åkerman Karl E.O., "Determination of the Intracellular Free Chloride Concentration in Rat Brain Synaptoneurosomes using a Chloride-sensitive Fluorescent Indicator", *Biochimica et Biophysica Acta (BBA) – Biomembranes*, 1993, 1153, 262–266.



### ***Chapter 3: Ultratrace level SERS simultaneous determination of Cu(II) and Co(II)***

---

#### **Abstract**

Independent and simultaneous SERS sensing of two environmental metallic pollutants, Cu(II) and Co(II) is presented throughout this chapter. The transition metal ions show high tendency to form coordination complexes with a terpyridine (TPY) derivative, used as the Raman sensitive probe. Alterations in the SERS vibrational pattern of the dithiocarbamate anchored terpyridine (TPY-DTC) in the presence of the metal ions were directly described as a function of the metal ion nature and concentration. As a further step we demonstrated the simultaneous ultradetection of Co(II) in the presence of high Cu(II) concentration, proposing this sensing strategy for monitoring potable water supplies.

### 3.1 Introduction

For healthy living organisms trace quantities of some of the heavy metals such as iron, copper, manganese, and zinc, are essential. They show high tendency towards organic ligands of biological matter containing nitrogen, sulfur, and oxygen provoking changes of the molecular structure inhibiting this way any biological functionality.<sup>1,2</sup> Heavy metals are responsible for toxicological and carcinogenic effects such as those affecting the central nervous system ( $\text{Hg}^{+2}$ ,  $\text{Pb}^{+2}$ ,  $\text{As}^{+3}$ ), the kidneys or liver ( $\text{Cu}^{+2}$ ,  $\text{Cd}^{+2}$ ,  $\text{Hg}^{+2}$ ,  $\text{Pb}^{+2}$ ) or skin, bones, or teeth ( $\text{Ni}^{+2}$ ,  $\text{Cu}^{+2}$ ,  $\text{Cd}^{+2}$ ,  $\text{Cr}^{+3}$ ). Additionally, they are not biodegradable and display an accumulative character in ecological systems and in the food chain causing high pollution levels. On account of such a risk, safe limits or maximum contaminant levels have been defined for drinking water by different organizations worldwide.<sup>34</sup>

Trace heavy metal sensing for the early detection of the pollution in the environment, including the living systems, attracts growing interest for the development of new and more effective sensing strategies.<sup>1,3</sup> Such sensing strategies should take under consideration the receptor that is responsible for the degree of selectivity and the immobilization/transducing platform which will depend on the technique used. Well established techniques for trace heavy metal analysis down to the ppt and ppq regime, are: atomic absorption spectroscopy (AAS), inductively coupled plasma-mass spectrometry (ICP-MS), mass spectroscopy (MS), X-ray fluorescence spectroscopy (R-FS), and potentiometric methods.<sup>1,4,5,6,7,8</sup> On the other hand, advances in the nanofabrication, such as the controlled synthesis of noble metal nanoparticles of various sizes and morphology, along with strategies based on optical methods, allow miniaturization of the sensing devices, enhance selectivity and sensibility, and can be rapid and cost-efficient.

SERS spectroscopy is proven to be an ultrasensitive analytical tool with the ability to allow easy rapid detection in complex media, without sample pretreatment protocols.<sup>9,10,11</sup> SERS detection lies in the uniqueness of the vibrational pattern of the analyte under study. However, SERS is not able to detect directly monoatomic species due to the absence of vibrational signatures, unless, they are chemically bound to a plasmonic substrate fashioned with the adequate receptors. SERS metal ion detection can be achieved either by binding to an organic receptor ligand, whose SERS profile can be modulated by formation of a coordination complex,<sup>11,12,13,14</sup> or by indirect detection using metal nanoparticles fashioned with Raman reporters whose SERS intensities are selectively perturbed by complexation of the target ions,<sup>15</sup> or by direct

adsorption onto the plasmon-active surface.<sup>16</sup> Characteristic intense SERS signals arise upon interaction of different ions with chemoselective receptors bound to plasmonically active substrates, offer the potential for multiplex detection.<sup>17</sup> Moreover the organic ligands can serve as internal standards that ensure the reliability of the SERS sensing platform and the analytical range of response can be easily controlled by varying the amount of chemoreceptor available on the metal surface.<sup>11</sup>

In the context of this chapter, we propose a simultaneous metal-ion SERS detection method based on the high affinity of two metal pollutants, Cu(II) and Co(II) to form coordination complexes with TPY moieties. Terpyridines are particularly appealing ligands because they bind metal ions through Raman-active pyridine units.<sup>11,18,19,20</sup> For a given terpyridine (TPY) structure, the conformation and electronic structure of the ligand–metal complex depends strongly on the metal ion species. Furthermore, the TPY binding site can be easily oriented toward the bulk solution for the easy capture of metal ions by introducing, a dithiocarbamate (DTC) unit at the opposite end of the TPY moiety, which serves as a robust anchoring group on the noble metal substrates.<sup>11,18,21</sup> The limits of detection by SERS spectroscopy of the two metals, Cu(II) and Co(II), can reach the ppb and ppt regime respectively.

## 3.2 Experimental details

### 3.2.1 Chemicals

All chemicals were purchased from Aldrich and used without further purification. Water was purified using a Milli-Q system (Millipore). 4'-(N-piperazinyl)terpyridine (pTPY) was synthesized as previously reported,<sup>18,22</sup> by condensing 4'-chloro-terpyridine with piperazine in 2,6-lutidine 5 for 24 h at 130 °C in a sealed reaction tube. pTPY was converted to the corresponding dithiocarbamate salt (TPY-DTC) by treatment with 1 equivalent each of CS<sub>2</sub> and Et<sub>3</sub>N in 1:1 CH<sub>2</sub>Cl<sub>2</sub>:MeOH, and used without further purification (final TPY-DTC concentration = 0.5 mM).

### 3.2.2 Nanoparticle synthesis and functionalization.

Ag nanoparticles were prepared via the method reported by Lee and Meisel.<sup>23</sup> Briefly, 2 mL of 1 wt% sodium citrate solution was added to 100 mL of a 1 mM solution of AgNO<sub>3</sub> at reflux and stirred for 1 hour. The resulting colloidal solution was a turbid gray-green colour. For functionalization, the Ag nanoparticles were centrifuged for 10

min at 2200 rcf, then decanted and redispersed in ethanol (2.5 times the retentate volume) before treatment with a TPY-DTC solution in 1:1 CH<sub>2</sub>Cl<sub>2</sub>:MeOH (final TPY-DTC concentrations of 10<sup>-5</sup>, 10<sup>-6</sup> and 10<sup>-7</sup> M). TPY-DTC ligands were allowed to adsorb overnight onto the Ag nanoparticles. 500 µL of the as-prepared TPY-DTC nanoparticle dispersion was then added to aqueous solutions containing different amounts of Co(II) and Cu(II), and gently stirred for 3 hours. Afterwards, 40 µL of the colloidal mixture was cast, air-dried, and analyzed by SERS.

### 3.2.3 Computational analysis

The geometries of the ligand and metal complexes with several water molecules were optimized by density functional theory (DFT) using the B3LYP functional with 6-31+G\* basis set. Silver atoms were described by the LANLDZ effective core potential together with the corresponding basis set. Frequency and force constants were obtained to enable a detailed vibrational assignment. Near field enhancement calculations, i.e. the near field intensity normalized by the incident intensity, were performed by using a 3D formulation of the scattering equations performed by using a 3D formulation of the scattering equations with the Green method.<sup>24</sup>

### 3.2.4 Instrumentation

UV-vis-NIR spectra were recorded using an Agilent 8453 diode array spectrophotometer. Transmission electron microscopy (TEM) was carried out using a JEOL JEM 1010 microscope operating at an acceleration voltage of 100 kV. Raman and SERS experiments were conducted using a Renishaw InVia Reflex confocal microscope equipped with a 50 objective and a high resolution grating with 1200 grooves per cm for NIR wavelengths, additional band-pass filter optics, and a 2D-CCD camera. SERS spectra were acquired using 785 nm excitation with exposure times of 10 s.

## 3.3 Results and discussion

Figure 3.1.A. schematically represents 4'-(N-piperazinyl)terpyridine (pTPY) molecule in the absence and after coordination with the metal cation transitioning from a transoid to a cisoid conformation respectively. Terpyridine ligands tend to form stable, inert, directed yet reversible complexes under certain conditions with many of the transition metal ions and in particular here with Co(II) and Cu(II).<sup>11,25,26</sup> Their high



binding affinity is due to the  $d\pi-p\pi^*$  back-bonding between the pyridine rings and the chelated metal cation.<sup>27</sup> The electronic absorption profiles of the pTPY and its two coordination complexes along with the UV-vis extinction spectrum and the TEM image of silver nanoparticles used as the plasmonic substrate to perform the SERS experiments for the identification of the two metals that follows, are shown in figure 3.1.B. Complexes of TPY with different metal ions affect its photophysical properties and this is directly reflected in the spectra of all three species which exhibit an intense absorption band located at 280 nm due to the  $\pi-\pi^*$  transitions of the TPY chromophore. Both Cu(II)-pTPY and Co(II)-pTPY complexes display a slight red shift relative to the free ligand with band maximum at 283 and 282 nm respectively, along with the characteristic metal-to-ligand charge transfer bands, typical for TPY-transition metal complexes at 310, 339 nm for Cu and at 302, 360 nm for Co.<sup>26</sup>

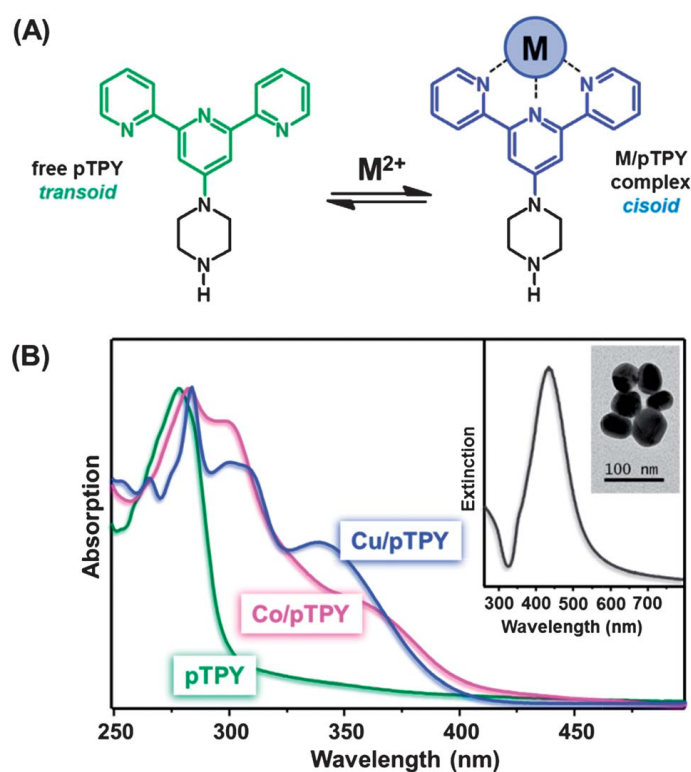


**Figure 3.1.** (A) Chemical structures of a free pTPY receptor and the one coordinated to a metal ion (green and blue respectively). (B) Normalized electronic absorption spectra of free pTPY and its equimolar Co(II) and Cu(II) complexes in 1 : 1 CH<sub>2</sub>Cl<sub>2</sub>-MeOH. Inset: A TEM image and an extinction spectrum of colloidal silver.

Next, in figure 3.2., are represented the Raman spectra of the pTPY moiety and its metal complexes, whose vibrational assignment was based on density functional theory (DFT) calculations. Theoretical calculations of the Raman spectra for the free and metal-bound pTPY ligand (prior to DTC functionalization) were performed to identify the vibrational contributions specific to the TPY unit. The spectral region at 1300-1650  $\text{cm}^{-1}$  holds similar changes of the TPY Raman bands upon complexation with Co(II) and Cu(II) and is characterized by a general broadening of the Raman peaks assignable to ring stretching modes and other in-plane deformations: 1606  $\text{cm}^{-1}$ , which is the result of several contributions ascribed to  $\nu(\text{CC})$  and  $\nu(\text{CN})$  ring modes of the three pyridine units; 1474  $\text{cm}^{-1}$ , due to a combination of a  $\nu(\text{CNC})$  in-plane ring and the CH in plane deformations; and a new band arising at 1324  $\text{cm}^{-1}$ , attributed to the CH rocking and the complex  $\nu(\text{CN})$  and  $\nu(\text{CC})$  inter- and intra-ring modes. However, in the 1200–1300  $\text{cm}^{-1}$  region, the intense sharp features of the free TPY ligand weaken to yield a single broad and weak band for Co–pTPY and Cu–pTPY approximately centered at 1243  $\text{cm}^{-1}$ .

The TPY Raman bands that by far concentrate the most prominent changes after metal coordination are observed in the ring-breathing bands at around 1000  $\text{cm}^{-1}$ . In the solid state, the doublet at 988 and 994  $\text{cm}^{-1}$  of the free pTPY ligand undergoes a notable shift upon complexation with Co(II) to give an intense peak centered at 1017  $\text{cm}^{-1}$ , with two visible shoulders at 1005 and 1028  $\text{cm}^{-1}$ . Coordination of the TPY moiety with Cu(II), also generates three well-resolved bands that are distinct from both free pTPY or Co(II)–pTPY, with the most intense peak at 1019  $\text{cm}^{-1}$  and two more at 997 and 1038  $\text{cm}^{-1}$ .

Identification of the metal–TPY-DTC complexes is accomplished due to the fact that all these differences in the solid-state Raman profiles of Co(II)–pTPY and Cu(II)–pTPY are also observed in the SERS spectra of these complexes. Additional contribution toward the distinction between Co(II)–TPY and Cu(II)–TPY is for instance that Cu(II) complexation produces several weak bands in the fingerprint region between 1064 and 1366  $\text{cm}^{-1}$  that are not present in either the free pTPY or Co(II)–pTPY Raman spectra.

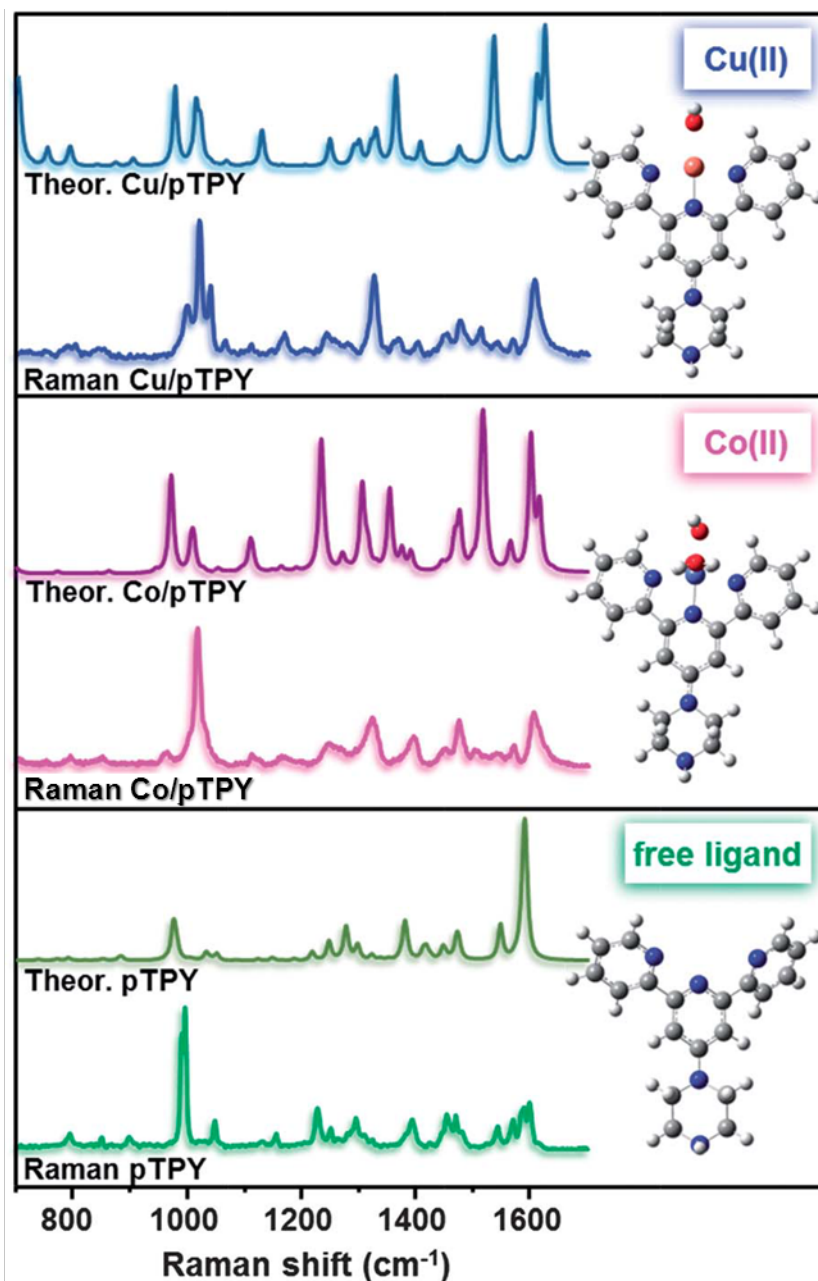


**Figure 3.2.** Comparison of theoretical and experimental (solid-state) Raman spectra of pTPY and its metal complexes. The geometries of pTPY and its complexes (with added water molecules) were optimized by DFT-B3LYP calculations using the 6-31+G\* basis set. Raman spectra were obtained using 785 nm excitation.

*Ultrasensitive SERS simultaneous determination of Cu(II) and Co(II)*

In order to improve the sensing efficiency of the SERS sensor, we first studied the effects of the ligand population over the metal surface at different surface coverages of self-assembled TPY-DTC receptors. Figure 3.3. shows the SERS spectra

of AgNPs treated with TPY-DTC solutions at concentrations ranging from  $10^{-5}$  to  $10^{-7}$  M, which is the practical sensitivity limit. At higher ligand concentrations, therefore at increased ligand density, results in significant spectral changes. In particular, the narrow ring-breathing mode at  $1019\text{ cm}^{-1}$  for TPY-DTC at  $10^{-7}$  M was split into a second contribution at  $995\text{ cm}^{-1}$ , and a new feature at  $1638\text{ cm}^{-1}$  arises in the spectral region characteristic of the  $\nu(\text{CN})$  and  $\nu(\text{CC})$  stretching modes. The conjugated  $\pi$ -system in TPY are significantly influenced by the ligand surface density, due to lateral interactions between molecules at high surface crowding altering structural and electronic properties, affecting its ability to coordinate to metal ions. Recently, Traulsen et al. showed that the amount of Pd(II) captured by a monolayer of TPY ligands on a metal substrate does not correlate well with the number of host binding sites but instead of that the metal coordination efficiency improves with a reduction in TPY density.<sup>28</sup> Given that,  $10^{-7}$  M was selected as the optimum TPY-DTC concentration for AgNP functionalization. In this point for the SERS metal ion detection was further optimized by also adjusting the AgNP concentration.

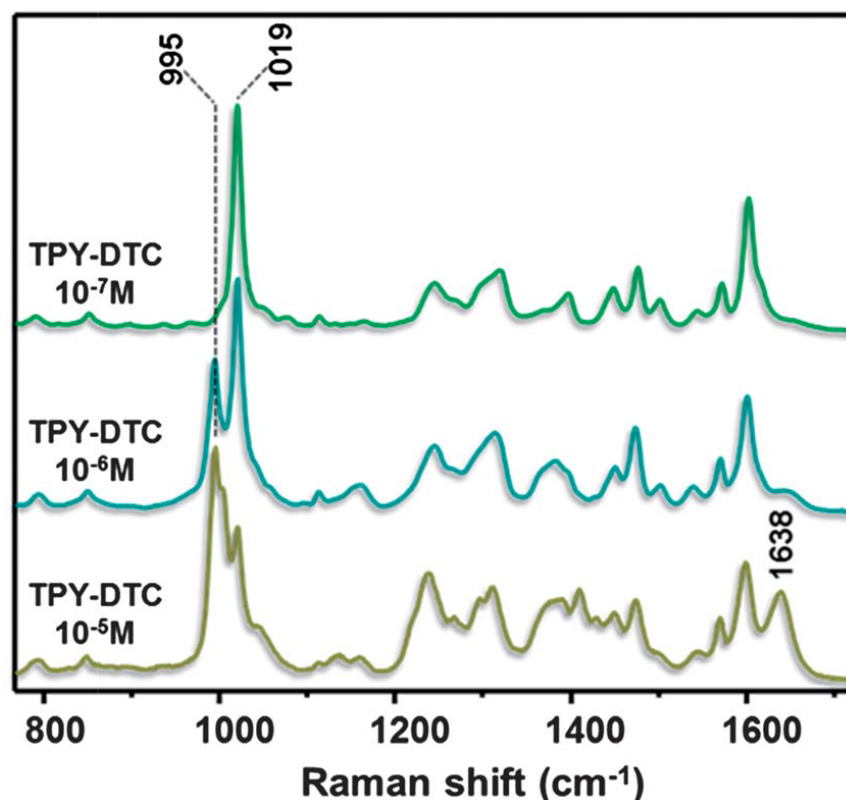


**Figure 3.3.** SERS spectra of TPY-DTC anchored onto Ag NPs as a function of free ligand concentration. Different aliquots of TPY solutions were added to a dispersion of Ag nanoparticles in ethanol ( $\sim 6 \times 10^{10}$  NPs per mL) until the desired final concentrations were obtained ( $10^{-5}$  to  $10^{-7}$  M). An aliquot of TPY-DTC-Ag NPs was diluted in deionized water before being cast, air-dried, and analyzed by SERS at 785 nm.

Prior to the SERS simultaneous detection of the Co(II) and Cu(II), we registered the SERS spectra of TPY-DTC–Ag NPs in the presence of varying amounts of the two metals individually as shown in figure 3.4. The coordination of metal ions to TPY-DTC ligands produced a general and non-specific red shift of several vibrational bands associated with in-plane ring vibrational modes, namely at 1318, 1474 and 1601  $\text{cm}^{-1}$ . The analyte-sensitive indicators of TPY complexation with Co(II) or Cu(II) were localized in the ring-breathing spectral region near 1000  $\text{cm}^{-1}$ . Concentrations of metal ions higher or lower than those reported in figure 3.4. did not induce any further change of the ligand spectral profile.

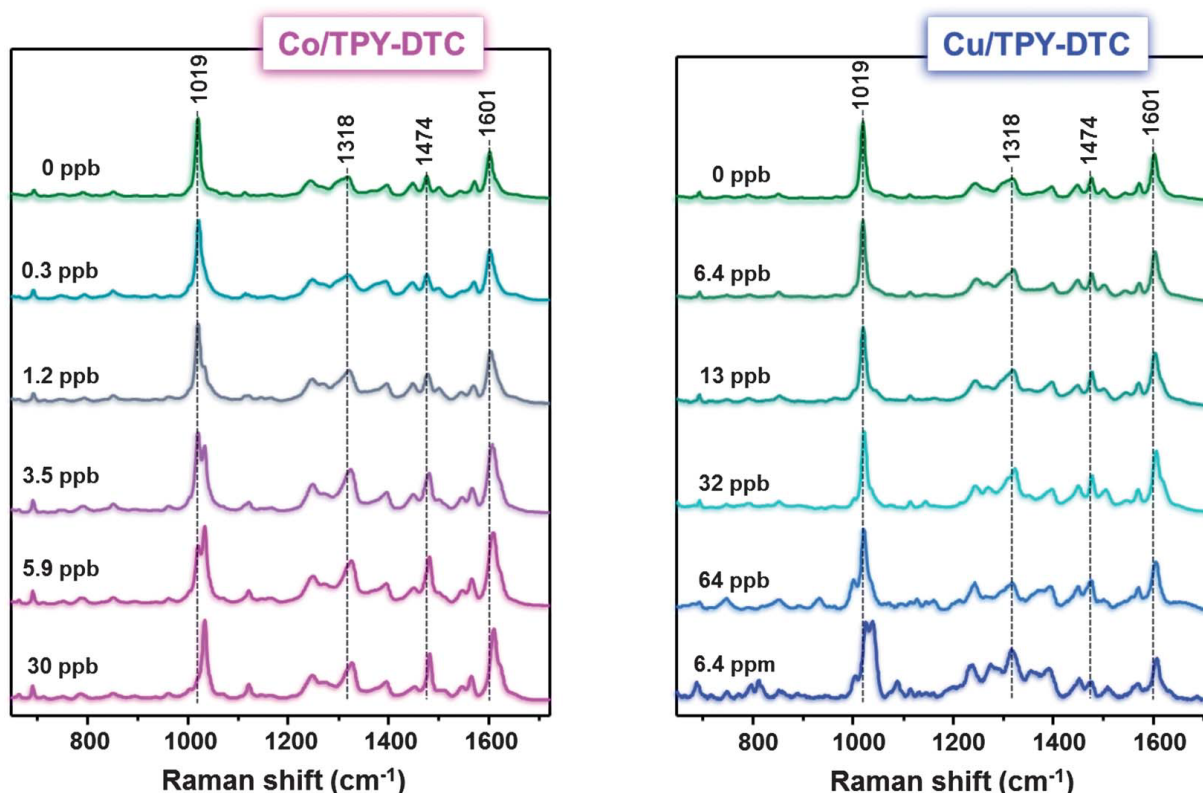


**Figure 3.4.** SERS spectra of TPY-DTC anchored onto Ag NPs at variable concentrations of  $\text{CoCl}_2$  and  $\text{CuCl}_2$ . AgNPs functionalized with TPY-DTC ( $10^{-7}$  M) were added to aqueous solutions containing different amounts of Co(II) and Cu(II) and gently stirred for 3 hours. 40 mL of each mixture was then cast, air-dried, and analyzed by SERS.

At relatively high metal ion concentrations (ppb levels), the vibrational peak of the metal–TPY-DTC complex ( $\nu_{\text{com}}=1033$   $\text{cm}^{-1}$  for Co(II), 1040  $\text{cm}^{-1}$  for Cu(II)) increases at the expense of the uncomplexed TPY vibrational mode ( $\nu_{\text{free}}=1019$   $\text{cm}^{-1}$ ) as represented in Figure 3.5.A. These changes were correlated quantitatively with metal

ion concentration using ratiometric peak intensities,  $I_{\text{com}}/I_{\text{free}}$ . Spectral peak deconvolution was performed for each Raman band between 1019 and 1040  $\text{cm}^{-1}$  at fixed FWHM values with the assumption of Lorentzian lineshapes.<sup>29</sup> In figure 3.5.B–D are shown the plots of  $I_{\text{com}}/I_{\text{free}}$  versus analyte concentration that reveal a linear correlation for both Co(II) and Cu(II) ( $r^2 > 0.97$ ) as shown. The detection limit is 6.5 ppb for Cu(II), and 60 ppt for Co(II). These experimental results suggest that the detection efficiency is of the same level or even lower than those obtained by widely accepted methods such as ICP (0.3 ppm for Cu) or FAAS (0.5 ppm for Cu, and 50 ppb for Co), and are competitive with ICP-MS (0.1 ppb for Cu, and 40 ppt for Co).<sup>34,35</sup>

Upon Co(II) addition a marked aggregation of TPY-DTC–AgNPs was observed, even at low analyte concentrations. Such a thing can be attributed to the supramolecular formation of bidentate  $[\text{Co}(\text{TPY})_2]^{2+}$  bridges between nanoparticles, as the stability constants for metal–TPY complexes increase with the degree of coordination ( $\beta_1(\text{Co–TPY}) > 10^8$ ,  $\beta_2(\text{Co–TPY}) > 10^{10}$ ).<sup>30,31,32</sup> This is also consistent with the observation that the colloidal solutions remain stable at higher Co(II) concentrations, due to the saturation of the TPY ligands. In contrast, nanoparticles were not destabilized by Cu(II), regardless of concentration. This result was again expected, since  $\beta_1(\text{Cu–TPY}) \sim \beta_2(\text{Cu–TPY}) \sim 10^8$ , permitting an exchange between non-bridging  $[\text{Cu}(\text{TPY})]^{2+}$  and bridging  $[\text{Cu}(\text{TPY})_2]^{2+}$  complexes.<sup>30</sup> The formation of the bidentate  $[\text{Co}(\text{TPY})_2]^{2+}$  bridges between nanoparticles generates uniform hot spots (interparticle separation  $\leq 2$  nm), selectively enhancing signals of the metal–ligand complexes within the interparticle gap where the highest electromagnetic fields are concentrated.<sup>33</sup> This accounts for the much higher sensitivity (nearly two orders of magnitude) of the TPY-based sensor for Co(II) detection as compared to Cu(II). The effect of localized electromagnetic fields on SERS signals is illustrated in figure. 3.5.E and F, where theoretical simulations of near-field intensity for a single AgNP and its homodimer (45 nm spheres, 2 nm gap,  $\lambda=785$  nm) are depicted.

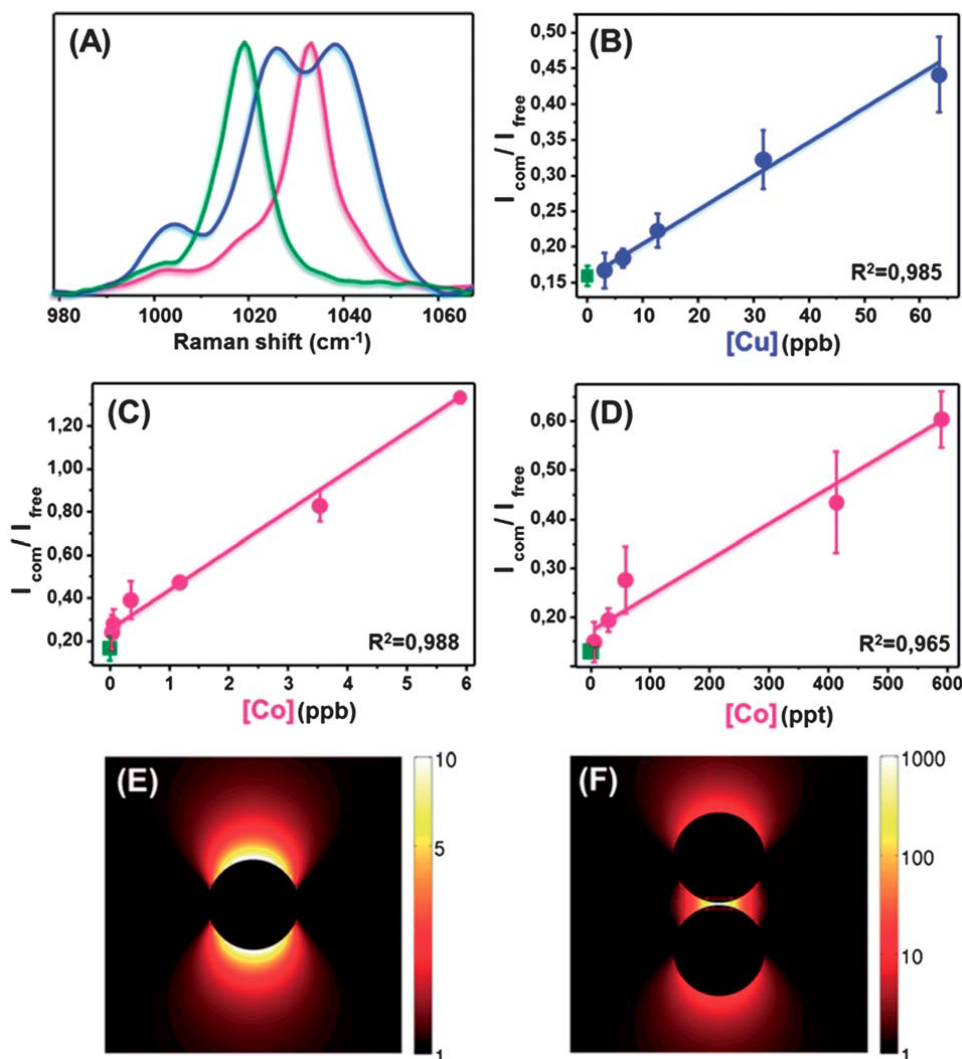


**Figure 3.5.** (A) Analyte-sensitive bands in the normalized SERS spectra of TPY-DTC in the absence of transition-metal ion (green line), in the presence of Co(II) (30 ppb, pink line), and in the presence of Cu(II) (6.4 ppm, blue line). (B)  $I_{com}/I_{free}$  as a linear function of [Cu], with a limit of detection at 6.5 ppb. (C and D)  $I_{com}/I_{free}$  as a linear function of [Co], with a limit of detection at 60 ppt. The concentration of TPY-functionalized AgNPs in sample (D) is ten times lower than in (B) and (C). Error bars equal to two standard deviations (N=5). (E and F). Near-field intensity maps (log<sub>10</sub> scale normalized to the incident field) for 45 nm AgNP spheres at 785 nm excitation: (E) a single Ag NP (F) a NP dimer with 2 nm gap.

The simultaneous detection of Co(II) and Cu(II) ions by TPY-DTC-AgNPs may be useful for monitoring potable water supplies. Recent drinking water standards recommend maximum concentrations for Cu(II) and Co(II) of 250 ppm and 20 ppb, respectively.<sup>36</sup> To demonstrate the ability of our SERS based method to detect ultratrace levels of Co(II) in the presence of high Cu(II) concentration, we designed an

experiment using mixtures of each metal ion in variable amounts. In figure 3.6 is represented the SERS readout from the TPY-DTC–AgNPs in the presence of Cu(II) and Co(II) at ppb levels. Most notably, SERS peaks corresponding to Co(II) adsorption can be distinguished at 0.6 ppb Co, and also in the presence of Cu(II) at a tenfold higher concentration. Similarly, Cu(II) can be detected in the presence of Co(II), but limited to a fivefold difference in concentration.

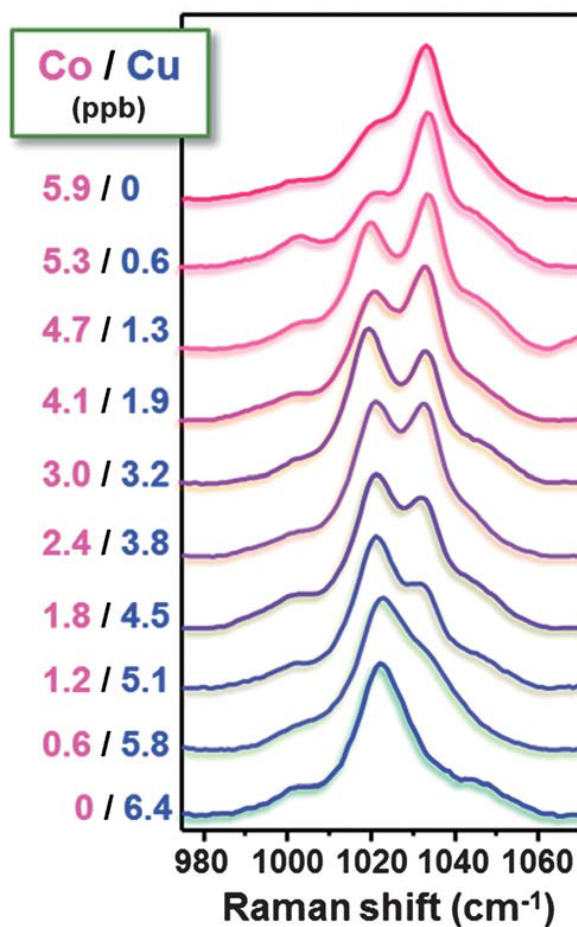


**Figure 3.6.** Analyte-sensitive SERS bands from TPY-DTC-AgNPs, after treatment with various mixtures of aqueous Co(II) and Cu(II) (listed in ppb).

### 3.4 Conclusions

In summary, we have engineered Ag nanoparticles into a quantitative, SERS-based sensor, using DTC-anchored terpyridine ligands with differentiating Raman spectral shifts in response to Co(II) and Cu(II). In the case of Co(II), the sensitivity of



the TPY-DTC-coated AgNPs toward these cations using SERS, was significantly higher than that provided by conventional analytical methods such as atomic absorption (or emission) spectroscopy. Further, the characteristic shifts in Raman peaks induced by each cation, make it possible to provide a simultaneous and independent assessment of Co(II) and Cu(II).

### 3.5 Bibliography

1. Aragay Gemma, Pons Josefina, and Merkoçi Arben, "Recent Trends in Macro-, Micro-, and Nanomaterial-Based Tools and Strategies for Heavy-Metal Detection" *Chemical Reviews*, 2011, 111, 3433–3458.
2. Haas Kathryn L. and Franz Katherine J., "Application of Metal Coordination Chemistry To Explore and Manipulate Cell Biology" *Chemical Reviews*, 2009, 109, 4921–4960.
3. Betts Kellyn S., "Technology Update: Heavy-metal Sensors Provide Fast Detection" *Environmental Science & Technology*, 1997, 31, 399A–399A.
4. Pohl Pawel, "Determination of Metal Content in Honey by Atomic Absorption and Emission Spectrometries" *TrAC Trends in Analytical Chemistry*, 2009, 28, 117–128.
5. Caroli S., Forte G., Iamicelli A.L., Galoppi G., "Determination of Essential and Potentially Toxic Trace Elements in Honey by Inductively Coupled Plasma-based Techniques" *Talanta*, 1999, 50, 327–336.
6. Flamini Riccardo and Panighel Annarita, "Mass Spectrometry in Grape and Wine Chemistry. Part II: The Consumer Protection" *Mass Spectrometry Reviews*, 2006, 25, 741–774.
7. Börjesson Jimmy and Mattsson Sören, "Medical Applications of X-ray Fluorescence for Trace Element Research" *Powder Diffraction*, 2007, 22, 130–137.
8. Mimendia Aitor, Legin Andrey, Merkoçi Arben and del Valle Manel, "Use of Sequential Injection Analysis to Construct a Potentiometric Electronic Tongue: Application to the Multidetermination of Heavy Metals", *AIP Conf. Proc.*, 2009, 1137, 420–426.
9. Alvarez-Puebla Ramon A. and Liz-Marzan Luis M., "Traps and Cages for Universal SERS Detection", *Chemical Society Reviews*, 2012, 41, 43–51.
10. Rodriguez-Lorenzo Laura, Fabris Laura, and Alvarez-Puebla Ramon A., "Multiplex Optical Sensing with Surface-enhanced Raman Scattering: A Critical Review", *Analytica Chimica Acta*, 2012, 745, 10–23.
11. Tsoutsis Dionysia, Guerrini Luca, Hermida-Ramon Jose Manuel, Giannini Vincenzo, Liz-Marzán Luis M., Wei Alexander and Alvarez-Puebla Ramon A.,

“Simultaneous SERS Detection of Copper and Cobalt at Ultratrace Levels”, *Nanoscale*, 2013, 5, 5841–5846.

12. Alvarez-Puebla Ramón A. and Liz-Marzán Luis M., “SERS Detection of Small Inorganic Molecules and Ions”, *Angewandte Chemie International Edition*, 2012, 51, 11214–11223.

13. Alvarez-Puebla R. A. and Liz-Marzán L. M., “Environmental Applications of Plasmon Assisted Raman Scattering”, *Energy & Environmental Science*, 2010, 3, 1011–1017.

14. Tsoutsis Dionysia, Montenegro Jose Maria, Dommershausen Fabian, Koert Ulrich, Liz-Marzán Luis M., Parak Wolfgang J., and Alvarez-Puebla Ramon A., “Quantitative Surface-Enhanced Raman Scattering Ultradetection of Atomic Inorganic Ions: The Case of Chloride”, *ACS Nano*, 2011, 5, 7539–7546.

15. Krpetić Željka, Guerrini Luca, Larmour Iain A., Reglinski John, Faulds Karen, Graham Duncan., “Importance of Nanoparticle Size in Colorimetric and SERS-Based Multimodal Trace Detection of Ni(II) Ions with Functional Gold Nanoparticles”, *Small*, 2012, 8, 707–714.

16. Wang G, Lim C, Chen L, Chon H, Choo J, Hong J, de Mello A.J., “Surface-enhanced Raman Scattering in Nanoliter Droplets: Towards High-sensitivity Detection of Mercury (II) Ions”, *Analytical and Bioanalytical Chemistry*, 2009, 394, 1827–1832.

17. Lee Seung Joon and Moskovits Martin, “Visualizing Chromatographic Separation of Metal Ions on a Surface-Enhanced Raman Active Medium”, *Nano Letters*, 2010, 11, 145–150.

18. Zhao Yan, Newton James N., Liu Jie, and Wei Alexander, “Dithiocarbamate-Coated SERS Substrates: Sensitivity Gain by Partial Surface Passivation”, *Langmuir*, 2009, 25, 13833–13839.

19. Laurence Ted A., Braun Gary B., Reich Norbert O., and Moskovits Martin, “Robust SERS Enhancement Factor Statistics Using Rotational Correlation Spectroscopy”, *Nano Letters*, 2012, 12, 2912–2917.

20. Goddard Gregory, Brown Leif O., Habbersett Robb, Brady Christina I., Martin John C., Graves Steven W., Freyer James P., and Doorn Stephen K., “High-Resolution Spectral Analysis of Individual SERS-Active Nanoparticles in Flow”, *Journal of the American Chemical Society*, 2010, 132, 6081–6090.

21. Guerrini Luca, Garcia-Ramos José V., Domingo Concepción, and Sanchez-Cortes. Santiago, “Sensing Polycyclic Aromatic Hydrocarbons with Dithiocarbamate-

Functionalized Ag Nanoparticles by Surface-Enhanced Raman Scattering”, *Analytical Chemistry*, 2009, 81, 953–960.

22. Clark M.L., Green R.L., Johnson O.E., Fanwick P.E., McMillin D.R., “DNA-binding and physical studies of Pt(4'-NR2-trpy)CN<sup>+</sup> systems (trpy = 2,2':6',2''-terpyridine)” *Inorganic Chemistry*, 2008, 47, 9410–9418.

23. Lee P. C. and Meisel D., “Adsorption and Surface-enhanced Raman of Dyes on Silver and Gold Sols”, *The Journal of Physical Chemistry*, 1982, 86, 3391–3395.

24. Giannini Vincenzo and Sánchez-Gil Jose A., “Calculations of Light Scattering from Isolated and Interacting Metallic Nanowires of Arbitrary Cross Section by Means of Green’s Theorem Surface Integral Equations in Parametric Form”, *Journal of the Optical Society of America A*, 2007, 24, 2822–2830.

25. Constable Edwin C., “2,2':6',2''-Terpyridines: From Chemical Obscurity to Common Supramolecular Motifs”, *Chemical Society Reviews*, 2007, 36, 246–253.

26. Hofmeier Harald, Hoogenboom Richard, Wouters Marielle E. L., and Schubert Ulrich S., “High Molecular Weight Supramolecular Polymers Containing Both Terpyridine Metal Complexes and Ureidopyrimidinone Quadruple Hydrogen-Bonding Units in the Main Chain”, *Journal of the American Chemical Society*, 2005, 127, 2913–2921.

27. Andres P.R. and Schubert U.S., “New Functional Polymers and Materials Based on 2,2':6',2''-Terpyridine Metal Complexes”, *Advanced Materials*, 2004, 16, 1043–1068.

28. Traulsen Christoph H.-H., Darlatt Erik, Richter Sebastian, Poppenberg Johannes, Hoof Santina, Unger Wolfgang E. S., and Schalley Christoph A., “Intermixed Terpyridine-Functionalized Monolayers on Gold: Nonlinear Relationship Between Terpyridyl Density and Metal Ion Coordination Properties”, *Langmuir*, 2012, 28, 10755–10763.

29. Thomas G.J. and Agard D.A., “Quantitative Analysis of Nucleic Acids, Proteins, and Viruses by Raman Band Deconvolution”, *Biophysical Journal*, 1984, 46, 763–768.

30. Dobraza Rainer, Lysetska Marina, Ballester Pablo, Grüne Matthias, and Würthner Frank, “Fluorescent Supramolecular Polymers: Metal Directed Self-Assembly of Perylene Bisimide Building Blocks”, *Macromolecules*, 2005, 38, 1315–1325.

31. Yam Vivian Wing-Wah, Wong Keith Man-Chung, and Zhu Nianyong, “Solvent-Induced Aggregation through Metal•••Metal/ $\pi$ ••• $\pi$  Interactions: Large Solvatochromism

of Luminescent Organoplatinum(II) Terpyridyl Complexes”, *Journal of the American Chemical Society*, 2002, 124, 6506–6507.

32. Lohmeijer Bas G. G. and Schubert Ulrich S., “Supramolecular Engineering with Macromolecules: An Alternative Concept for Block Copolymers”, *Angewandte Chemie International Edition*, 2002, 41, 3825–3829.

33. De Boeck Marlies, Kirsch-Volders Micheline, and Lison Dominique, “Cobalt and Antimony: Genotoxicity and Carcinogenicity”, *Metals and Human Cancer*, 2003, 533, 135–152.

34. World Health Organization, “Guidelines for drinking-water quality”, 2008.

35. World Health Organization, “Cobalt and Inorganic Cobalt Compounds Concise International Chemical Assessment Document 69”, 2006.

36. Sustainable Water Group, Water Quality Guidelines, [http://www.bsr.org/reports/awqwg/BSR\\_AWQWG\\_Guidelines-Testing-standards.pdf](http://www.bsr.org/reports/awqwg/BSR_AWQWG_Guidelines-Testing-standards.pdf), 2010.



## ***Chapter 4: General Conclusions***

---

In the context of the present research project, we have reached the following general conclusions:

1. We have successfully designed and produced a novel SERS-based sensor for the ultradetection of chloride.
  - The excellent sensing efficiency of the sensor lies upon the remarkable SERS intensity, arising from the plasmon coupling between silver nanoparticles, formed all over the surface of a micrometer-sized silica bead, that acts as a stable platform. Such a hybrid material offers a stable substrate for the Raman reporter, with a dense collection of hot spots and overcomes colloidal stability issues.
  - The other key element of the sensor is the Raman reporter itself. This agent is required to selectively interact with the analyte under study and undergoes significant vibrational change upon exposure. The vibrational response of the Cl-sensitive probe molecule was studied and exploited to devise a remote, indirect SERS sensor with the ability of selectively identifying and quantifying minute amounts of chloride, even down to the picomolar regime.

Such a SERS sensing strategy of halides, opens new ways of possibilities and applications. For example, since only chloride is present in the cytosol of cells, we anticipate this kind of sensor to be of key importance in the study of molecular and metabolic processes in living biological systems.

2. We propose a quantitative SERS method of independent and simultaneous determination of two metals, Cu(II) and Co(II), which are of environmental concern.
- Silver nanoparticles are used as the optically active substrate to perform successfully qualitative and quantitative SERS experiments. We use DTC-anchored terpyridine ligands with distinct vibronic response to Co(II) and Cu(II), that is correlated as a function of each metal ion concentration, with limits of detection comparable to those of several conventional analytical methods.
  - We demonstrate simultaneous detection of ultratrace levels of Co(II) in the presence of high Cu(II) concentration. Each one of the two cations, interacts differently with the terpyridine moiety, inducing characteristic shifts in Raman signals.

Simultaneous trace sensing exploiting SERS methodologies, of two metal pollutants such as Cu(II) and Co(II), are of great interest. Although both Cu(II) and Co(II) are bioessential trace elements, they are toxic at high concentrations. Over time, the long-term exposure of organisms to low amounts of these metal ions can result in bioaccumulation of toxic levels, potentially promoting teratogenic or carcinogenic effects. Consequently, such a SERS-based strategy can provide a reliable, fast and quantitative monitoring of natural waters with a potential multiplex capability.



## ***List of Publications***

This research work is related to the following publications:

- Tsoutsi Dionysia, Montenegro Jose Maria, Dommershausen Fabian, Koert Ulrich, Liz-Marzán Luis M., Parak Wolfgang J., and Alvarez-Puebla Ramon A., “Quantitative Surface-Enhanced Raman Scattering Ultradetection of Atomic Inorganic Ions: The Case of Chloride” *ACS Nano*, 2011, 5, 7539–7546.
- Tsoutsi Dionysia, Guerrini Luca, Hermida-Ramon Jose Manuel, Giannini Vincenzo, Liz-Marzán Luis M., Wei Alexander and Alvarez-Puebla Ramon A., “Simultaneous SERS Detection of Copper and Cobalt at Ultratrace Levels”, *Nanoscale*, 2013, 5, 5841–5846.







